Clonal-aggregative multicellularity entrained by salinity in one of the closest relatives of animals

Núria Ros-Rocher[1*], Josean Reyes-Rivera[2*], Uzuki Horo[1], Chantal Combredet[1], Yeganeh Foroughijabbari[1], Ben T. Larson[2,3], Maxwell C. Coyle[2], Erik A.T. Houtepen[4], Mark J. A. Vermeij[4,5], Jacob L. Steenwyk[2], Thibaut Brunet[1+]

[1]Institut Pasteur, Université Paris-Cité, CNRS UMR3691, Evolutionary Cell Biology and Evolution of Morphogenesis Unit, 25-28 Rue du Dr. Roux, 75015 Paris, France

[2]Howard Hughes Medical Institute and the Department of Molecular and Cell Biology, University of California, Berkeley, Berkeley, CA, USA

[3]Present address: Department of Biochemistry and Biophysics, University of California, San Francisco, San Francisco, CA, USA

[4]Caribbean Research and Management of Biodiversity foundation (CARMABI), Piscaderabaai z/n Willemstad, Curaçao

[5]Department of Freshwater and Marine Ecology, Institute for Biodiversity and Ecosystem Dynamics, University of Amsterdam, Amsterdam, 1012 WP, The Netherlands

*Contributed equally

+Lead contact

Correspondence: N. R.-R.: nuria.ros@pasteur.fr J. R.-R.: josean.reyes@berkeley.edu T.B.: thibaut.brunet@pasteur.fr

Multicellularity evolved multiple times independently during eukaryotic diversification[1–4]. Two distinct mechanisms underpin multicellularity[5]: clonal development (serial cell division of a single precursor cell) and aggregation (in which independent cells assemble into a multicellular entity). Clonal and aggregative development are traditionally considered mutually exclusive[1,6–9], and evolutionary hypotheses have addressed why multicellular development might diverge toward one or the other extreme[3,4]. Both animals and their sister group, the choanoflagellates, are currently thought to only develop clonally[10,11], apparently supporting an exclusively clonal pre-history for animal multicellularity[4,12]. Here, we show that the choanoflagellate *Choanoeca flexa*, one of the closest living relatives of animals[13], develops into motile and contractile monolayers of cells (or "sheets") through an unexpectedly mixed, plastic mechanism: *C. flexa* sheets can form by purely clonal processes, purely aggregative processes, or a combination of both. We characterize the life history of *C. flexa* in its natural environment, ephemeral splash pools on the island of Curaçao, and show that multicellular development is controlled by salinity during natural cycles of splash pool evaporation and refilling. Different splash pools house genetically distinct strains of *C. flexa* between which aggregation is constrained by kin recognition, a hallmark of aggregative multicellularity[14–17]. We propose that clonal-aggregative development allows fast and reversible transitions between unicellular and multicellular lifestyles in this rapidly fluctuating environment. Our findings challenge former generalizations about the choanoflagellate-animal lineage and expand the option space for the development and evolution of multicellularity.

Multicellularity has evolved independently over 45 times across eukaryotes[18], with multiple independent origins of both clonal and aggregative multicellularity[7,19]. Efforts to reconstruct the origin of animal multicellularity have benefited from the study of their closest living relatives: the choanoflagellates (**Figure 1A**)[20–23]. Choanoflagellates are bacterivorous aquatic microeukaryotes bearing an apical flagellum surrounded by a collar of interconnected actin-filled microvilli (**Figure 1B-C**)[24]. Moreover, many choanoflagellate species display facultative multicellular development[24–28]. As in animals, multicellular development is clonal in all choanoflagellate species investigated thus far[25,29–31], which contrasts with the occurrence of aggregative multicellularity in more distantly related lineages, such as filastereans[32–35] and dictyostelid amoebae[36,37]. These observations, together with the clonal nature of animal embryogenesis, have inspired the hypothesis that animals evolved from organisms with a

simple form of clonal multicellularity, akin to that observed in certain modern choanoflagellates and in other close relatives of animals such as ichthyosporeans[38–40].

Here, we describe an unusual type of multicellular development in the colonial choanoflagellate *Choanoeca flexa*[41], that challenges previous generalities about choanoflagellates. We report that *C. flexa* colonies develop by a combination of clonal and aggregative development, which we refer to as 'clonal-aggregative multicellularity'. We propose that this unusual mode of development represents an adaptation to the dynamic natural environment of *C. flexa*: splash pools that undergo extreme salinity fluctuations during natural cycles of evaporation and refilling.

C. flexa sheets can develop clonally

C. flexa was discovered in 2018 in the form of concave monolayers of polarized cells (or "sheet colonies"; **Figure 1A-D**) held together through direct collar-collar adhesions[41,42]. *C. flexa* sheets are capable of inverting their curvature under the control of environmental cues, thus switching from a feeding state (relaxed form, flagella-in; **Figure 1B**) to a swimming state (contracted form, flagella-out; **Figure 1D**)[41,43]. In an earlier study, we established stable cultures of *C. flexa* sheets from a single isolated cell, indicating that sheets can arise from individual cells[41]. Nevertheless, the mechanisms of *C. flexa* multicellular development remained unexplored.

To understand *C. flexa* colony development, we first isolated and monitored single cells from mechanically disassembled sheets by time-lapse microscopy. In this context, we observed clonal development of sheets by serial cell division (**Figure 1E-F; movie S1**): cells divided asynchronously every ~8-10 hours and sister cells remained attached to each other by intermicrovillar contacts. This resulted in a monolayer of polarized cells with the signature curved morphology of *C. flexa* sheets (**Figure 1E-F; movie S1**). These observations show that small *C. flexa* sheets (up to 7 cells) can develop clonally from a single cell. To test whether clonal development can contribute to the further growth of *C. flexa* colonies, we monitored small and medium-sized colonies (from 6 to 46 cells) by time-lapse microscopy and regularly observed clonal expansion by cell division both at the core and periphery of the sheets (**Figures 1G and S1; movies S2-S3**). However, unexpectedly, we also captured instances of free-swimming single cells and doublets meeting colonies, attaching to their periphery, re-orienting to align their apico-basal axis with neighboring cells, and seemingly integrating into

96 the sheet (**Figures 1G and S1; movies S2-S3**). Taken together, these results show that *C.*
97 *flexa* colonies can form clonally but might also be able to expand by aggregation. This
98 motivated us to test whether *C. flexa* could also acquire multicellularity purely by aggregation
99 (**Figure 1H**).
100
101 ## *C. flexa* sheets can develop by aggregation
102
103 To test whether *C. flexa* colonies can form by aggregation, we mechanically disassembled
104 colonies into free-swimming single cells and performed live imaging of the dissociated cells
105 (**Figure 2A-B; movie S4**). We found that *C. flexa* single cells aggregated within minutes into
106 irregular masses of cells that continued incorporating additional cells and underwent repeated
107 fusion into larger groups (*i.e.* agglomeration[44]; **Figure 2B; movie S4**). To determine the fate
108 of these aggregates, we labeled two populations of dissociated single cells with different
109 fluorophores. After mixing both populations, cells of both colors aggregated within minutes
110 (**Figure S2A; movie S5**). After 24 hours, we observed chimeric colonies displaying the
111 polarized cup-shaped morphology typical of canonical *C. flexa* sheets and comprising cells of
112 both colors (**Figures 2C and S2B-C; movies S6-S8**), indicating that they had developed by
113 aggregation. To better understand the dynamics of aggregative development, we fixed
114 aggregates at different stages and imaged them by Airyscan confocal microscopy. We found
115 that early aggregates (up to 6 hours post-dissociation (hpd)) displayed a variable and irregular
116 morphology with cells frequently showing unaligned apico-basal polarity, likely resulting from
117 collision and attachment of cells in diverse random orientations (**Figures 2D and S3; movies**
118 **S9-S12**). Colonies observed 24 hpd, on the other hand, were regular polarized monolayers of
119 cells (**Figures 2D and S3; movie S13**), suggesting that early irregular aggregates had
120 matured into canonical sheets.At that stage, colonies comprised about 50 cells on average
121 and as many as 120 cells (**Figure 2E**). This size further supported the idea that these sheets
122 could not have formed exclusively by clonal development within 24 hours, given the cell cycle
123 duration in *C. flexa* (at least 8 hours (**Figure 1F**), which could result in sheets comprising at
124 most 16 cells assuming maximal and synchronized proliferation). Indeed, treatment with the
125 cell cycle inhibitor aphidicolin abolished cell proliferation (**Figure S4A**) but did not affect colony
126 formation from dissociated cells (**Figure 2F and S4B**), confirming that aggregation was
127 sufficient for *C. flexa* multicellular development.
128

129 Our observation of aggregative development in *C. flexa* contrasts with earlier observations
130 in other species of multicellular choanoflagellates, which have so far been found to develop
131 strictly clonally[24–26]. Given that other protists often deploy aggregative development as an
132 "emergency response" to fluctuating environments[3,45], while clonal development is thought to
133 be more frequent in environments sufficiently stable to sustain cell proliferation, we were
134 curious about the natural conditions of *C. flexa* mixed clonal-aggregative development. Thus,
135 we set out to investigate the life history of *C. flexa* in its natural environment.
136

137 **Occurrence of multicellular *C. flexa* in the field is limited by salinity**

138

139 *C. flexa* was originally discovered in its multicellular form on the tropical island of
140 Curaçao[41] (**Figure 3A**). Unlike other multicellular choanoflagellate species[21,46], *C. flexa* has
141 been repeatedly re-isolated in the field since its discovery in 2018 and can thus be studied in
142 its native biotope. *C. flexa* sheets are found on the windward northern part of the island in
143 splash pools (**Figures 3A-B and S5A-B**) that undergo natural cycles of desiccation and
144 refilling[47,48]. Water-filled splash pools experience gradual evaporation, leading to increasing
145 salinity and, occasionally, complete desiccation (**Figure 3C**). Splash pools refill from crashing
146 waves, splash, or rain, restoring lower salinity levels (**Figures 3C and S5B; movie S14**). As
147 a consequence, splash pools are ephemeral habitats in which organisms experience extreme
148 and recurrent hypersaline and hyperosmotic stress[48–51]. We set out to investigate how this
149 environment might influence the life history and multicellular development of *C. flexa*.
150 We focused our studies on Shete Boka National Park, where *C. flexa* is reliably found
151 (**Figure 3A**). We surveyed the distribution of *C. flexa* in 150 splash pools and measured splash
152 pool salinity in two different field expeditions: Exped-A and Exped-B (**Figure 3D**). During
153 Exped-A, we sampled 79 splash pools (numbered Sp1 to Sp79) along about 2 kilometres of
154 coastline (**Figure 3D**; see methods). While seawater collected from the neighbouring inlets
155 (or *bokas*) had a stable salinity of ~40 parts per thousand (ppt), splash pool salinity ranged
156 from below average seawater salinity (15 ppt) to saturation (≥ 280 ppt) (**Figures 3E and S5D**).
157 In 10 out of 79 splash pools, we found choanoflagellate sheets that exhibited the
158 stereotypical *C. flexa* cup-shaped morphology and inversion behaviour in response to light-
159 to-dark transitions[41] (**Figures 3F and S6A-C; movie S15 and Table S1**). 18S ribosomal DNA
160 sequencing of manually isolated sheets confirmed their identification as *C. flexa* (**Figure S6D;**
161 **supplementary files S1-S4**). Interestingly, although the salinity of surveyed splash pools
162 ranged from 15 to 280 ppt, *C. flexa* sheets were only found in splash pools with <94 ppt salinity

(**Figures 3E and S5D; Table S1**). To independently test whether the presence of multicellular *C. flexa* was constrained by an upper salinity limit, we exhaustively sampled all splash pools (n=71, numbered M1 to M71; **Figure 3D' and S5C**) within a 4-meter by 10-meter quadrant in a second expedition (Exped-B). We found sheets in 14 out of 71 splash pools, with a 128 ppt salinity upper bound for sheet occurrence (**Figures 3E and S5D**). Across both expeditions, *C. flexa* sheets were found in splash pools with an average salinity of 61.5±23.7 ppt, 1.56-fold that of natural seawater (**Figures 3E and S4C**) and significantly lower than splash pools that did not contain sheets (155.1±107.2 ppt; p=3.1e-04 by the Mann-Whitney U test). We never observed sheets in splash pools with a salinity above 128 ppt (3.2-fold seawater; **Figures 3E and S5D; Table S1**).

Multicellular development is entrained by evaporation-refilling cycles in nature

We then set out to study how the natural evaporation-refilling cycle of splash pools impacts the presence/absence of sheets. We monitored ten splash pools in which *C. flexa* sheets were found on Day 1 and five more randomly selected splash pools daily over eight days (**Figures 3G-H and S7**). We measured salinity and maximum depth and screened samples for sheets once per day (**Figures 3G-H and S7**). We observed a gradual decrease in depth and increase in salinity in all 15 splash pools (presumably due to evaporation; **Figure S7A-B**), six events of complete desiccation (**Figure S7C-D**), and four events of refilling (**Figure S7E-F**; see three examples in **Figure 3H**). In all cases, *C. flexa* sheets were no longer observed after salinity crossed a ~120 ppt threshold during gradual evaporation (**Figures 3H and S7**), consistent with results from Exped-A and Exped-B (**Figures 3E-H and S7**). Moreover, evaporation in the laboratory of a natural splash pool sample containing sheets led to sheet disappearance (**Figure S8**). These observations confirmed that the multicellular form of *C. flexa* does not tolerate high salinity.

Interestingly, in two dry splash pools that underwent refilling during our study (restoring salinity down to ~50 ppt), sheets were observed 48 hours after refilling (Sp69 and Sp70; **Figures 3H and S7E-F**). The newly observed sheets may have arrived from the ocean or from neighbouring splash pools. Alternatively, *C. flexa* might have persisted in the soil of desiccated splash pools in a cryptic resistant form, such as unicellular cysts (described in other choanoflagellates[52–57]). Under this hypothesis, colonies would disassemble and differentiate into resistant single cells under high salinity, and those cells would then develop back into sheets once salinity decreased. To explore this possibility *in situ*, we collected soil

197 samples from seven desiccated splash pools in which *C. flexa* had been previously observed,
198 rehydrated them in the lab (down to ~65 ppt salinity) and monitored the rehydrated samples
199 for several days (**Figure 3I-K; movie S16 and Table S1**). Sheets were recovered from various
200 soil samples collected from two splash pools after two to seven days of desiccation in the field
201 (**Figure 3I-K and Table S1**). Sheets were consistently observed 48-72 hours after rehydration
202 in the laboratory, suggesting that a resistant form of *C. flexa* can survive complete desiccation
203 (**Figure 3I-K and Table S1**). Interestingly, earlier metagenomic analyses of diverse
204 environments had suggested that choanoflagellates might often be present in soil[58,5960].
205 Given that salinity fluctuations in splash pools seemed to dramatically impact *C. flexa*
206 multicellularity in nature, we next set out to investigate the phenotypic response of *C. flexa* to
207 comparable evaporation-refilling cycles in a laboratory context.
208

209 **Multicellular development is entrained by evaporation-refilling cycles in the**
210 **laboratory**

211

212 We designed an experimental setup mimicking the natural evaporation-refilling cycles of
213 Shete Boka splash pools (**Figures 4A-C and S9A**). We subjected *C. flexa* cultures to
214 evaporation in an incubator (**Figure 4A**), approximating the temperature (30°C) and
215 evaporation rate of natural splash pools (see methods; **Figure 4B-C and S9A**). Starting from
216 the standard salinity of artificial seawater (ASW; 35 ppt, hereafter referred to as 1X salinity),
217 this setup resulted in complete desiccation after four days of evaporation. Under these
218 conditions, *C. flexa* sheets gradually dissociated into non-motile single cells (**Figures 4D-E**
219 **and S9B; movie S17**), with more than 50% solitary cells when salinity crossed the natural
220 limit of sheet occurrence (128 ppt; **Figures 3E and 4AD**. Almost all sheets had dissociated
221 into single cells when salinity reached saturation (**Figures 4D-E and S9B; movie S17**). By
222 contrast, control cultures without evaporation remained multicellular throughout the
223 experiment (**Figure S9C**). Finally, to directly test whether loss of multicellularity was due to
224 increased salinity, we added seawater salt to *C. flexa* cultures (without evaporation) and
225 similarly observed dissociation of multicellular sheets into single cells (**Figure S10A-C**).
226 We then tested whether single cells resulting from sheet dissociation were viable and
227 could survive desiccation. We rehydrated samples by adding artificial seawater three hours
228 after desiccation, thus mimicking refilling by waves. This brought salinity back down to ~50
229 ppt and was followed by the reappearance of sheets as soon as 24 hours post-rehydration as

230 well as by a continuous increase in the number of colonies over the following days (**Figure**
231 **4D-E**).
232 We assessed the mechanism of colony re-formation by time-lapse microscopy of
233 desiccated cultures after rehydration and captured instances of unicellular flagellates
234 engaging in both clonal and aggregative multicellular development (**Figure S9D; movie S18**).
235 Taken together, our results show that *C. flexa* sheets dissociate into non-motile single cells
236 during gradual evaporation, that these solitary cells can survive complete desiccation, and
237 that sheets reform after rehydration through both clonal division and aggregation. These
238 findings are consistent with our field observations, where we recovered sheets after
239 rehydrating soil samples from a dry splash pool (**Figure 3I-K and Table S1**), and further
240 support the existence of a desiccation-resistant form of *C. flexa*.
241
242 ***C. flexa* sheets dissociate and differentiate into unicellular cysts at high salinity**
243
244 We set out to further investigate the phenotype of desiccation-induced single cells. In
245 diverse protists, resistance to desiccation is often achieved by differentiation into cysts[61–63],
246 *i.e.* dormant cells with reduced metabolic activity and minimal or arrested proliferation.
247 Encystation often entails significant morphological changes such as rounding of the cell body,
248 changes in cell volume, flagellar loss, and formation of a protective cell wall [55,61,64–70]. We
249 monitored cellular morphology by DIC microscopy during gradual evaporation and observed
250 structural changes that occurred asynchronously, resulting in a heterogeneous cell population
251 (**Figure 4F-I**). At 3X salinity, most cells had dissociated from their colonies and bore a round
252 cell body without microvilli and often without flagellum (**Figure 4G-I**). Additionally, some cells
253 exhibited filopodia-like protrusions (**Figure 4G-H**). Membrane and F-actin staining of
254 desiccation-resistant cells (hereafter 'cysts') confirmed that they lacked a collar complex
255 (**Figures 4J-L and S11**) but also revealed that a transient F-actin cortex, detectable at 3X
256 salinity but lost above 6X (close to saturation; **Figures 4K-L and S11**). This cortex might
257 contribute to protecting the plasma membrane against osmotic stress during early
258 differentiation[71–74].
259 Next, we determined whether *C. flexa* cysts actively proliferate by quantifying cell growth
260 during gradual evaporation in the laboratory. We found that growth was arrested above 2X
261 salinity, with net cell loss above 3X salinity (**Figures 4M and S12**). These effects may be
262 attributable to a halt in the cell cycle and cell death due to hypersaline stress, similar to
263 changes observed during encystation in other protists[36,61,64,70,75].

264 Finally, morphometric analysis of cell body and nucleus volume showed that cysts had a
265 larger nucleus-to-cytoplasm ratio compared to flagellates in 1X salinity (p=3.4e-05; **Figures**
266 **4N and S13**). An increase in the nucleus-to-cytoplasm ratio frequently correlates with cell
267 quiescence[76], consistent with the growth arrest in *C. flexa* cysts (**Figures 4M and S12**). To
268 confirm that these changes were induced by hypersaline stress, we directly increased the
269 salinity of *C. flexa* cultures by addition of seawater salt and observed similar morphological
270 changes and arrest in cell growth (**Figure S10**).
271 The suite of drastic and reversible cellular changes induced by hypersalinity in *C. flexa*
272 (**Figure 4O**) resembles encystation in diverse other protists[61,64]. During the natural
273 evaporation-refilling cycle of a splash pool, *C. flexa* thus likely alternates between a
274 multicellular flagellated form (at low salinity) and a unicellular cyst-like form (at high salinity),
275 suggesting these two phenotypes each confer an adaptive advantage in their respective
276 environment. We therefore directly tested these putative advantages in laboratory conditions.
277

278 **Multicellular sheets and unicellular cysts are respectively advantaged at low**
279 **and high salinity**

280

281 If *C. flexa* cysts represent a desiccation-resistant form, we could expect these cells to be
282 more resistant than sheets to hypersaline stress and desiccation. To test this, we induced the
283 differentiation of *C. flexa* into cysts by slow evaporation following the protocol detailed in the
284 previous section (from 1X salinity to desiccation in 72 hours). In parallel, we subjected sheets
285 to fast evaporation, causing desiccation over 20 hours from 1X salinity (see methods). Under
286 these conditions, cells did not acquire a cyst-like morphology but instead retained an
287 observable flagellum, collar, and multicellular morphology even when completely desiccated
288 (**Figure S14**). This observation suggests that the formation of cysts requires gradual
289 evaporation at a comparable rate to that of natural splash pools. After desiccation, we
290 rehydrated both types of cells by adding 1X ASW and monitored their recovery. We found that
291 desiccated sheets having undergone rapid evaporation never developed into viable cells after
292 rehydration (**Figure 4P**). By contrast, as in the experiments detailed earlier, rehydrated cysts
293 consistently gave rise to viable sheets (**Figure 4P**). These observations show that cysts,
294 unlike flagellates, are equipped to survive hypersalinity and desiccation, and suggest that
295 encystation confers a selective advantage during evaporation. The loss of multicellularity
296 during encystation is likely due to the retraction of microvilli, that connects cells within sheet
297 colonies.

298

299 We further wondered whether multicellularity, by contrast, was advantageous in the other
300 phase of the cycle, marked by low salinity. It has been speculated that multicellularity in
301 choanoflagellates might enhance feeding via cooperative hydrodynamic interactions between
302 flagella[77–79], although attempts to test this hypothesis in the model choanoflagellate
303 *Salpingoeca rosetta* have yielded conflicting results[77,80,81]. To test for a feeding advantage in
304 multicellular *C. flexa* sheets, we quantified the capture of fluorescent bacteria in sheets and
305 dissociated single flagellates (**Figure 4Q-R**). We found that sheets captured more than twice
306 as many fluorescent bacteria per cell as single cells (**Figure 4Q-R**). This suggests that
307 multicellularity confers a prey capture advantage at the low salinity level compatible with
308 maintenance of a functional collar complex, and therefore with feeding.

309

310 ## *C. flexa* cell density in natural splash pools is sufficient for aggregation

311

312 We next challenged our model by testing whether aggregative development can plausibly
313 occur in the natural context of Curaçao splash pools. A pre-requirement for aggregation is
314 sufficient cell density, as cells need to be at above a minimum concentration to encounter
315 each other and aggregate. We quantified *C. flexa* cell density in 12 splash pools and found
316 that cell density ranged from 30 to $4.4*10^4$ cells/mL. 5/12 splash pools had a higher estimated
317 cell density than the minimum density used in laboratory aggregation experiments (from
318 $1.0*10^4$ to $6.7*10^5$ cells/mL). Thus, *C. flexa* can be present in nature in sufficient density to
319 allow aggregation.

320

321 ## Aggregation is constrained by kin recognition

322

323 To further assess the relevance of aggregation to the life history of *C. flexa*, we decided
324 to test for additional biological signatures of aggregation. A frequent feature of aggregative
325 multicellularity is kin recognition – *i.e.* the ability to discriminate kin versus non-kin, thereby
326 restricting aggregation to closely related strains. This is classically interpreted as an
327 adaptation to restrict the spread of cheater mutants[15]. We set out to test kin recognition
328 between three *C. flexa* strains: the one used in laboratory experiments above (Strain 1,
329 originally isolated in 2019) and two additional strains isolated in 2023 during Exped-B, Strains
330 2 and 3 (**Figure 5B-C**). Each strain was independently isolated from a different splash pool

331 by manual isolation of a single sheet colony followed by amplification in laboratory cultures
332 (resulting in "single-sheet-bottlenecked" cultures). Several clonal lines were established from
333 each strain by single-cell bottlenecking.

334 To test for genetic divergence between these strains, we first sequenced, assembled and
335 annotated the reference *C. flexa* genome by a combination of long-read and Omni-C
336 sequencing. The final assembly comprised 56 MB and 14,084 genes across 528 scaffolds,
337 with a BUSCO completeness score of 82.8%. This represents the third high-quality
338 choanoflagellate genome after *M. brevicollis* and *S. rosetta*[82,83]. We then performed short-read
339 sequencing of Strains 1, 2 and 3, as well as of three clonal (single-cell-bottlenecked)
340 descendants for each strain. 193,564 SNPs were detected with high confidence across all
341 samples, allowing us to reconstruct a phylogenomic tree in which all three parent strains were
342 clearly delineated from each other (**Figure 5D and supplementary files S5-S6**). All single-
343 cell-bottlenecked clones clustered with their strain of origin with high support, indicating
344 significant genetic divergence between strains but little to no diversity within strains. Single-
345 sheet-bottlenecked cultures contained a similar amount of genetic diversity as single-cell-
346 bottlenecked clones (**Figure S16**). The latter suggests either clonal development of the
347 originally isolated sheets (as in **Figure 1E-G**) or loss of genetic diversity during sheet isolation
348 and establishment of laboratory cultures (see Methods).

349 We then tested whether aggregation between strains was constrained by kin recognition.
350 We dissociated sheets of all three strains, stained them with different fluorophores, and
351 assessed aggregation between all pairwise combinations of strains (seeded at equal initial
352 cell density, as in **Figure 2C**). All strains aggregated into sheets within hours, confirming
353 aggregation as a widespread behavior in newly isolated strains. Interestingly, cells of Strains
354 1 and 2 preferentially aggregated with their own strain when combined, indicating kin
355 discrimination (**Figure 5E-H and S15**). By contrast, other pairwise combinations of strains
356 showed no quantifiable preference for cells of the same strain and readily aggregated into
357 chimeric sheets (as did cells of the same strain stained with different fluorophores, consistent
358 with earlier results; **Figure 2C**).

359 These results suggested the existence of a kin recognition system in *C. flexa*, similar to
360 those described in other aggregative multicellular organisms such as dictyostelid social
361 amoebae. In the latter, kin recognition is mediated by polymorphic surface receptors rich in
362 immunoglobulin domains and other adhesion domains[17,84]. In *Dictyostelium*, kin recognition
363 receptors were originally identified by their high ratio of non-synonymous to synonymous
364 substitutions (dN/dS), a signature of diversifying selection[17]. We reasoned that, if *C. flexa*

365 indeed possesses a kin recognition mechanism, candidate kin recognition loci might be
366 revealed by screening the genomes of Strain 1 and Strain 2 for high dN/dS loci. We identified
367 466 genes with high dN/dS ratio regions, that encoded predicted proteins with a significant
368 overrepresentation of domains consistent with an adhesion (immunoglobulin, cadherin, EGF,
369 fibronectin, HYR) or a signaling (protein tyrosine phosphatase, SH2 domain) function (**Figure**
370 **5I-K**). Many of these genes additionally encoded predicted transmembrane domains, with
371 adhesion domains on the extracellular side and signaling domains on the cytoplasmic side
372 (**Figure 5J-K**). This shows that multiple polymorphic receptors potentially mediating kin
373 recognition can readily be identified between diverse *C. flexa* strains, although some of these
374 proteins might perform other functions (such as capture of bacterial prey). Determining their
375 function will require functional genetic tools, that currently do not exist for *C. flexa*.
376
377 Taken together, our findings support a model of *C. flexa* life history that correlates with the
378 evaporation-refilling cycle of splash pools characteristic of their natural habitat (**Figure 6**). *C.*
379 *flexa* sheets are found in water-filled splash pools with salinities below ~3-fold that of natural
380 seawater. As gradual evaporation proceeds, salinity increases, and sheets dissociate and
381 differentiate into solitary, non-motile, and non-proliferative cysts (some of which undergo cell
382 death). These cysts can survive complete desiccation and persist in the soil of the splash
383 pools. After splash pool refilling, cysts regrow a collar complex and transition back into free-
384 swimming flagellates that develop into multicellular sheets by aggregation and/or clonal
385 division, a phenotype that more efficiently captures bacteria and presumably supports faster
386 cell proliferation.
387
388 **Discussion**
389
390 Our results show that *C. flexa* can form multicellular sheets through a combination of
391 clonal division and aggregation following the rehydration of desiccated cysts. This mixed
392 developmental strategy might represent an adaptation to the ephemeral nature of splash
393 pools, allowing faster multicellular development by simultaneous action of both mechanisms.
394 Indeed, one key advantage of aggregation is speed: across eukaryotes,
395 aggregativemulticellular forms often complete multicellular development from a unicellular
396 state in only a few hours[19,19,85]. By contrast, estimates of the duration of the cell cycle in nature
397 (that constrains the speed of clonal development) for diverse micro-organisms range from
398 one to eleven days (**Table S3**). The clonal-aggregative multicellularity of *C. flexa* might thus

399 serve as a versatile strategy for robust establishment of multicellularity across a broad range
400 of environmental conditions: indeed, aggregative and clonal multicellularity are subjected to
401 different constraints, as they respectively depend on cell density and on the possibility of cell
402 division (the latter, in turn, being constrained by salinity and availability of bacterial prey). In
403 our laboratory experiments, *C. flexa* appeared capable of both purely clonal development (at
404 low cell density and under stable permissive conditions for proliferation) and purely
405 aggregative development (at sufficient cell density, even if proliferation is compromised), as
406 well as intermediate modes.

407 The environmentally entrained life history transitions of *C. flexa* are in line with other
408 recently described examples. Unicellular-to-multicellular switches are controlled by fluctuating
409 environmental parameters in other species, such as salinity for cyanobacteria in brackish
410 environments[86] and periodic flooding for cave bacteria attached to surfaces[87]. A selective
411 advantage for regulated life cycles in fluctuating environments has also been supported by
412 laboratory experiments in yeast[88] and by theoretical models[5,89,90]. The phenotypic plasticity of
413 *C. flexa* might thus enable it to reap both the benefits of multicellularity (for feeding and
414 collective behavior) under permissive conditions, and of differentiation into solitary cysts for
415 individual survival under harsh conditions.

416 The selective advantage of multicellularity has been actively debated[78,91–93] including
417 in choanoflagellates[77,78,94–98]. In *C. flexa*, the prey capture efficiency of cells within sheets
418 surpasses that of solitary flagellated cells, suggesting a feeding (and likely reproductive)
419 benefit of multicellularity. Indeed, cooperative feeding is observed among various protists and
420 has been postulated as a selective factor for the evolution of multicellularity[99]. However,
421 multicellularity might confer other advantages to *C. flexa.* For example, collective contractility
422 underlying whole-colony inversion allows emergent behaviors such as photokinesis
423 (preferential accumulation of sheets under light), which has been shown to require
424 multicellularity[41]. Yet another advantage might be decreased vulnerability to size-selective
425 predators, as described in other protists[19,78,92,100] (but see [97]).
426

427 The clonal-aggregative multicellularity of *C. flexa* contrasts with that of previously
428 characterized multicellular choanoflagellates, which appear to develop solely clonally[24,26,101–
429 103] – the best-characterized example being the development of rosette colonies in *S. rosetta*[26].
430 Beyond choanoflagellates, both clonal and aggregative multicellularity are widely present, with
431 a discontinuous occurrence, across unicellular holozoans[2,25] and eukaryotes as a whole[25,104–
432 106]. The scattered distribution of clonal and aggregative multicellularity is currently interpreted

433 as reflecting independent evolutionary origins of both types of development[3]. However, the
434 discovery of clonal-aggregative multicellularity in a choanoflagellate raises the intriguing
435 alternative possibility of evolutionary interconversions between aggregative and clonal
436 multicellular development (via a mixed intermediate). Indeed, clonal-aggregative
437 multicellularity might be more widespread than currently appreciated. Notably, clonality and
438 aggregation have been proposed to cooperate in the formation of diverse structures across
439 prokaryotes and eukaryotes, including bacterial biofilms[107], experimentally evolved clusters of
440 bacteria[108], predator-induced groups of freshwater algae (which can even combine different
441 species)[109], and unicellular, but multinucleated syncytia in reticulopodial amoebae[18]. Although
442 these diverse processes might not all represent *bona fide* multicellular development[110] (as the
443 resulting structures seem to lack controlled shape, size, or collective behavior), they show that
444 cell division and aggregation behaviour can coexist.
445
446 Aggregative multicellularity comes with a well-known evolutionary challenge: one
447 aggregate can combine cells of different ancestries and potentially different genotypes, thus
448 raising the possibility of conflict[111–113]. Aggregates are notably vulnerable to cheater
449 genotypes, which reap the benefits of multicellularity without contributing their fair share of the
450 cost of multicellular development. Such cheaters have for example been described in
451 *Dictyostelium*[114], *Myxococcus*[115], and in flocculating yeast[116]. The difficulty of resolving such
452 conflicts, alongside that of coordinating complex functions in aggregates potentially combining
453 multiple genotypes[19], might limit the evolutionary potential of aggregative multicellularity.
454 Indeed, all five eukaryotic lineages with "complex multicellularity" (*i.e.* controlled three-
455 dimensional morphogenesis and spatial cell differentiation), including animals, fungi, and land
456 plants, develop clonally rather than by aggregation[25,117], and aggregative multicellular forms
457 instead tend to be transient and facultative[116–120]. Aggregative development often occurs in
458 conditions where the benefit of fast development outweighs the cost of potential genetic
459 conflict – either because adverse conditions make cell proliferation (and therefore clonal
460 development) infeasible[19,36,121] or because fast multicellular development is required as an
461 "emergency response" to acutes stress[19,116,122]. Indeed, aggregative multicellularity is
462 frequently induced by stressors such as nutrient depletion[36,45] or presence of
463 predators[100,121,123]. In such situations, aggregation allows for rapid establishment of a
464 multicellular structure that confers a selective advantage (*e.g.* increased size, shielding of
465 inner cells, or elevation from the substrate by formation of a stalk). Often, the endpoint of
466 stress-induced aggregative multicellularity is the formation of a fruiting bodiy: a mass of non-

467 proliferative cells that disperses into single cells before resuming metabolic activity and
468 proliferation (as described in dictyostelid amoebae[3,45,124], multiple other eukaryotes[125,126], and
469 myxobacteria[127]). Interestingly, and by contrast, *C. flexa* sheets, although they similarly
470 develop under time pressure, are proliferatively and behaviorally active. Thus, the ecological
471 niche of mixed clonal-aggregative multicellularity might differ from that of typical aggregative
472 forms.
473
474 Nonetheless, the risk posed by cheaters can be addressed by strategies that limit
475 aggregation to fellow co-operators, either directly by co-operator recognition (so-called "green
476 beard" mechanisms[128,129]) or indirectly by preferential aggregation with close relatives.
477 Restriction of aggregation to relatives can either be enforced actively by kin recognition
478 (usually mediated by polymorphic loci[130–132]) or be facilitated passively by spatial structuration
479 of the environment that can limit dispersal[133,134]. The latter mechanism might also be relevant
480 to *C. flexa*, as splash pools are collections of physically disconnected environments that might
481 lead to geographic divergence of genotypes (as shown for other organisms in similar
482 environments, such as *Daphnia* metapopulations in tide pools[135]). Splash pools might thus
483 favor the evolution of aggregative multicellularity by initially relaxing the need for strong kin
484 recognition mechanisms (which *C. flexa* nonetheless displays). This is in line with recent
485 models proposing an “ecological scaffolding” function for patchy environments in the
486 emergence of multicellularity[136]. In the future, deeper characterization of molecular kin
487 recognition mechanisms, natural genetic diversity and dispersal in *C. flexa* might shed further
488 light on these questions.
489
490 The complex life history of *C. flexa* illustrates the phenotypic and developmental
491 plasticity of close unicellular relatives of animals and thus lends additional support to the
492 emerging concept of a pre-metazoan origin for complex life cycles[20,137]. Beyond this, our study
493 establishes *C. flexa* as a model to study the facultative multicellular development of a close
494 relative of animals in its natural context. This contrasts with other well-characterized
495 facultatively multicellular holozoans, such as *S. rosetta*[21] and *C. owczarzaki*[138], which could
496 both be isolated only once from their natural environment and in which studies of unicellular-
497 to-multicellular transitions are thus inevitably restricted to laboratory settings. In the future, we
498 expect the dialogue between field and lab studies of *C. flexa* to continue, clarifying questions
499 such as the selective advantage(s) and ecological implications of multicellularity and
500 unicellularity, as well as the mechanism of kin recognition.

Data availability

The annotated reference *C. flexa* genome has been deposited on Zenodo under doi: 10.5281/zenodo.13837466. Raw short reads for Strains 1, 2 and 3 have been deposited on Zenodo under doi: 10.5281/zenodo.13837614.

Code availability

The codes used for SNP analysis are deposited on Github: https://github.com/uhoro/RRRR_SNP_analysis

Acknowledgements

We thank Nicole King for support during this project and for providing useful feedback. We thank the personnel of the Shete Boka National Park in Curaçao for access to the field site. Special thanks to Tess Linden for help during preliminary field experiments and feedback on the manuscript, as well as to Geneviève Milon and Noah Whiteman for advice on laboratory and field experiments, respectively. Yashraj Chavhan, Seemay Chou, and Stefania Kapsetaki provided useful feedback on the preprint version of the manuscript. Marvin Albert, Stéphane Rigaud and Jean-Yves Tinevez at the Image Analysis Hub at the Institut Pasteur provided advice on image analysis. Pierre-Henri Commere and Sebastien Megharba from the Flow Cytometry platform at Institut Pasteur provided technical support with single-cell isolation of *C. flexa* by flow cytometry. We acknowledge the help of the HPC Core Facility of the Institut Pasteur for bioinformatic analyses. We thank Thomas Swale (Dovetail Genomics/Cantata) and Tara Rickman (Phase Genomics) for help with genome sequencing and assembly and for drafting the relevant Methods sections. We also thank members of Brunet and King laboratories for feedback and useful discussions and Jaime Ramirez and Kayla Dinshaw for technical support during preliminary experiments. NRR is supported by the European Union's Horizon Europe research and innovation funding program under a Marie Skłodowska-Curie Actions grant (Grant Agreement ID: 101106415). JRR is supported by a National Science Foundation Graduate Research Fellowship Program (grant no. 1752814). UH is supported by the PPU program of the Institut Pasteur. Work in the King lab (TB, JRR, BTL, MCC) is supported by the Howard Hughes Medical Institute. JLS is a Howard Hughes Medical Institute Awardee of the Life Sciences Research Foundation. TB and work in the Brunet lab are supported by the Institut Pasteur (G5 package), the ERC (EvoMorphoCell, grant agreement ID 101040745), the Vallee Foundation Inc, and the CNRS (UMR 3691). Views and opinions expressed are, however, those of the author(s) only and do not necessarily reflect those of the European Union or the European Research Council. Neither the European Union nor the granting authority can be held responsible for them.

Author contributions

NRR, JRR, TB conceptualized the study and coordinated the work across coauthors. MCC, BTL and TB performed preliminary fieldwork that identified the Shete Boka site and gave first insights in the *C. flexa* salinity range. NRR, JRR and TB collected fieldwork data included in this study. NRR, JRR and TB performed all laboratory experiments, strain isolations and bioinformatic analyses (except those specified below). BTL performed preliminary aggregation assays and aphidicolin treatments. YF optimized live imaging of dual-labelling aggregation experiments and performed growth curves under addition of salts. JLS performed genome assembly and annotation. UH performed SNP analyses with technical guidance from JLS. CC performed single-cell bottleneck isolations and generated the material for genome sequencing of Strains 1, 2 and 3. EATH and MAV provided support for fieldwork studies.

EATH performed drone orthomap imagery. JRR wrote the first draft of the manuscript which was subsequently edited by NRR and TB. NRR made the figures with feedback from JRR and TB. TB supervised the study. All authors contributed to the review of the manuscript before submission for publication and approved the final version.

Inclusion & ethics statement

Local and regional researchers who supported or performed part of the Curaçao fieldwork are authors of the present manuscript.

Competing interests

JLS is an advisor for ForensisGroup Inc.

Materials and Methods

See detailed Materials and Methods in the **Supplementary Information** file.

Supplementary Material

Supplementary Figures S1-S16, Tables S2-S3 and legends for Table S1, Supplementary Files S1-S6 and Supplementary Movies S1-S18 are provided in the **Supplementary Information** file.

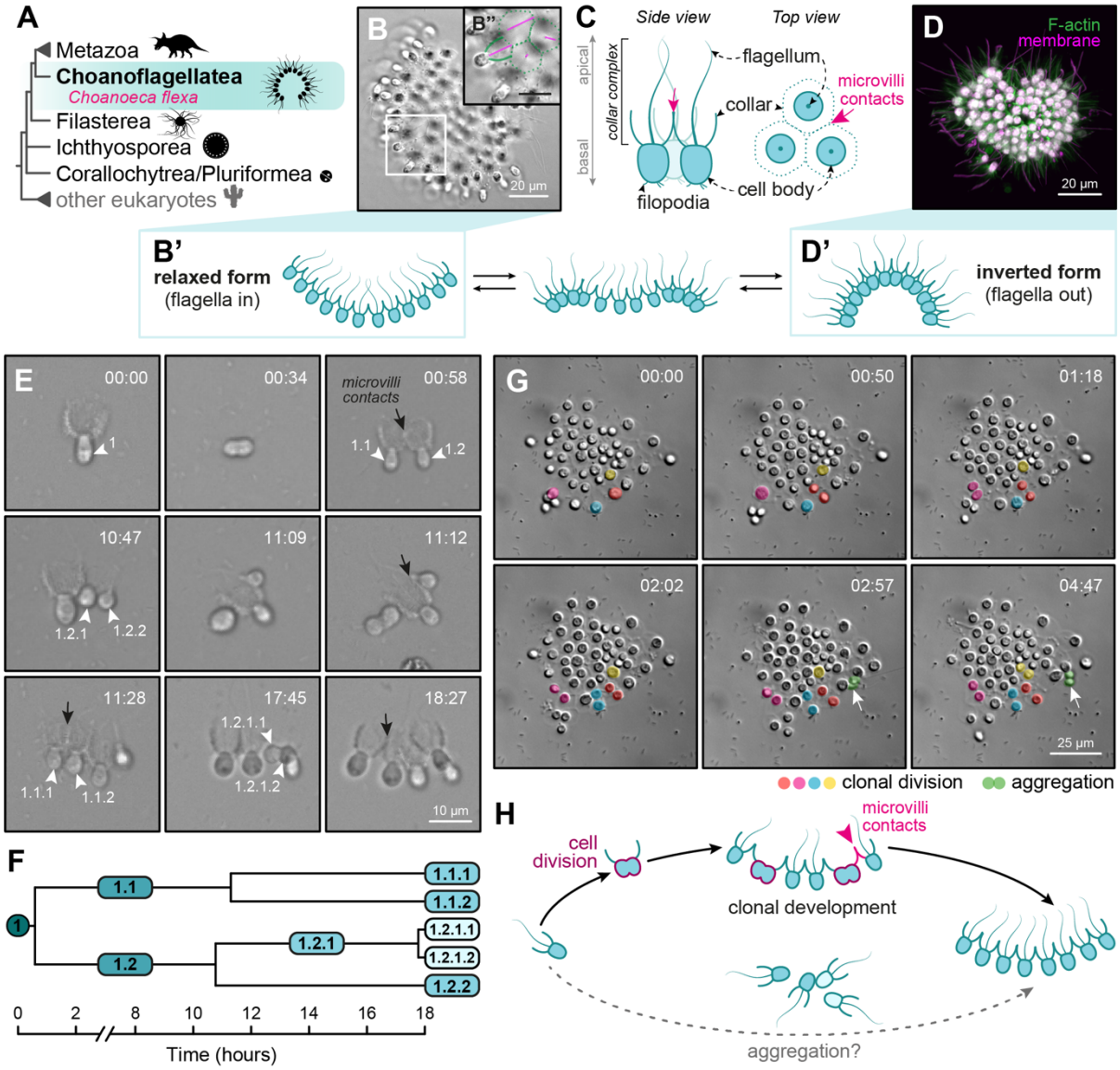

Figure 1. *Choanoeca flexa* sheets can develop clonally but display aggregative features.

(A) Choanoflagellates (turquoise) are the sister group to animals (Metazoa). The phylogenetic relationships depicted are based on several recent phylogenomic studies [25,27,32,41,139–142]. Uncertain positions are represented with polytomies. (B) Brightfield image of a *C. flexa* multicellular colony ("sheet") in its relaxed conformation (B'). B", white square: zoom-in showing flagella (magenta pseudocolor) and direct cell-cell contacts between collars (green pseudocolor). Scale bar in B'': 10 µm. (C) Diagnostic morphological features of a choanoflagellate cell. *C. flexa* cells within a sheet are linked by their collars (orange arrow). (D) 3D reconstruction of an Airyscan Z-stack of a fixed sheet exhibiting an inverted conformation (D'), with cell bodies stained with a membrane/cytoplasmic dye (FM™ 1-43FX, magenta, which distributes to the membrane and cytoplasm of cells following fixation), and microvilli stained with a filamentous actin (F-actin) dye (phalloidin Alexa 488, green). (E) Stills from a brightfield timelapse movie of clonal *C. flexa* sheet development by serial cell division from a single *C. flexa* swimmer cell (white arrowhead). After each division, the sister cells remain adhered to each other by direct cell-cell contacts between collars (black arrow). Note that cells retract their flagellum during

583 division. Time scale hh:mm. (F) Cell lineage tracing as a function of time in E shows that cells divide
584 asynchronously during colony formation, taking ~8-10 hours between each round of division. (G) Stills
585 from a brightfield timelapse movie depicting a medium-sized *C. flexa* sheet (flagella-in conformation)
586 that expands in cell number both by cell division (pseudocoloring in orange, pink, blue and yellow) and
587 by cellular aggregation (white arrow, pseudocoloring in green). Time scale hh:mm. (H) Schematics of
588 *C. flexa* clonal multicellular development observed under laboratory culture conditions: unicellular
589 flagellate (swimmer) cells can divide clonally to initiate a colony; in turn, colonies can increase in cell
590 number by clonal division, maintaining cell-cell contacts through direct adhesions in their collar (orange
591 arrowhead). The hypothesis that *C. flexa* sheets might be able to develop purely by aggregation is
592 tested in Figure 2. Figure related to **Figure S1** and **movies S1-S3**.
593

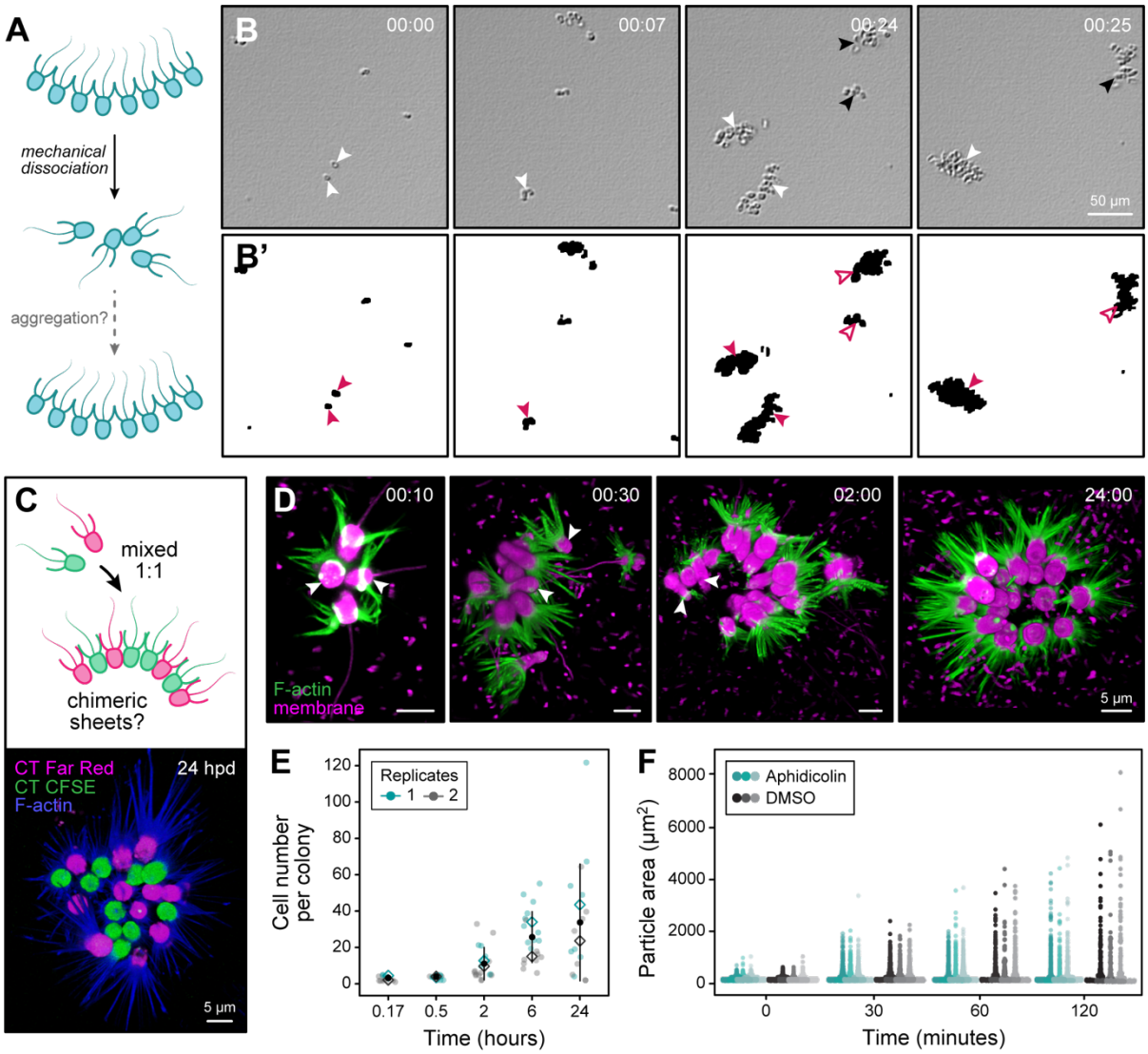

Figure 2. *C. flexa* can develop by aggregation.

(A) Schematics of the experimental assay to test *C. flexa* aggregation. Colonies are mechanically disassembled into free-swimming single cells and the resulting dissociated single cells are live imaged. (B) Stills from a brightfield timelapse movie showing that dissociated single cells (white arrowheads) quickly re-formed colonies by cellular aggregation. Note that two colonies can fuse together by agglomeration (black arrowheads). (B') Binary image mask of stills in B. Time scale hh:mm. (C) (Upper panel) Dissociated single flagellate cells labelled with Cell Trace CFSE (green) or Cell Trace Far Red (magenta) and mixed in a 1:1 ratio will form chimeric colonies 24 hours post-dissociation (hpd) if aggregation occurs. (Lower panel) 3D reconstructions of Airyscan Z-stacks of a sheet formed by aggregation from dissociated single cells labelled as depicted above and fixed 24 hpd, with additional filamentous actin (F-actin) staining (phalloidin Alexa 405, blue). (D) 3D reconstructions of Airyscan microscopy images of single cells fixed after 10 minutes (n=12), 30 minutes (n=12), 2 hours (n=19), and 24 hours (n=16) post-dissociation stained for membrane/cytoplasm (FM^{TM} 4-64FX, magenta) and F-actin (phalloidin Alexa 488, green). Note that cells frequently show unaligned apico-basal polarity and diverse cell orientations at early timepoints (white arrowheads). Time scale hh:mm. (E) Quantification of cell number per colony during aggregation (from the experiment in D) in two independent biological replicates. Black circles: mean. Error bars: standard deviation. Diamonds: mean

612 values of independent biological replicates. (F) Quantification of particle area during an aggregation
613 time course of dissociated single cells pre-treated with 17 µg/mL aphidicolin overnight in three
614 independent biological replicates. DMSO: negative control. Figure related to **Figures S2-S4** and
615 **movies S4-S13**.
616

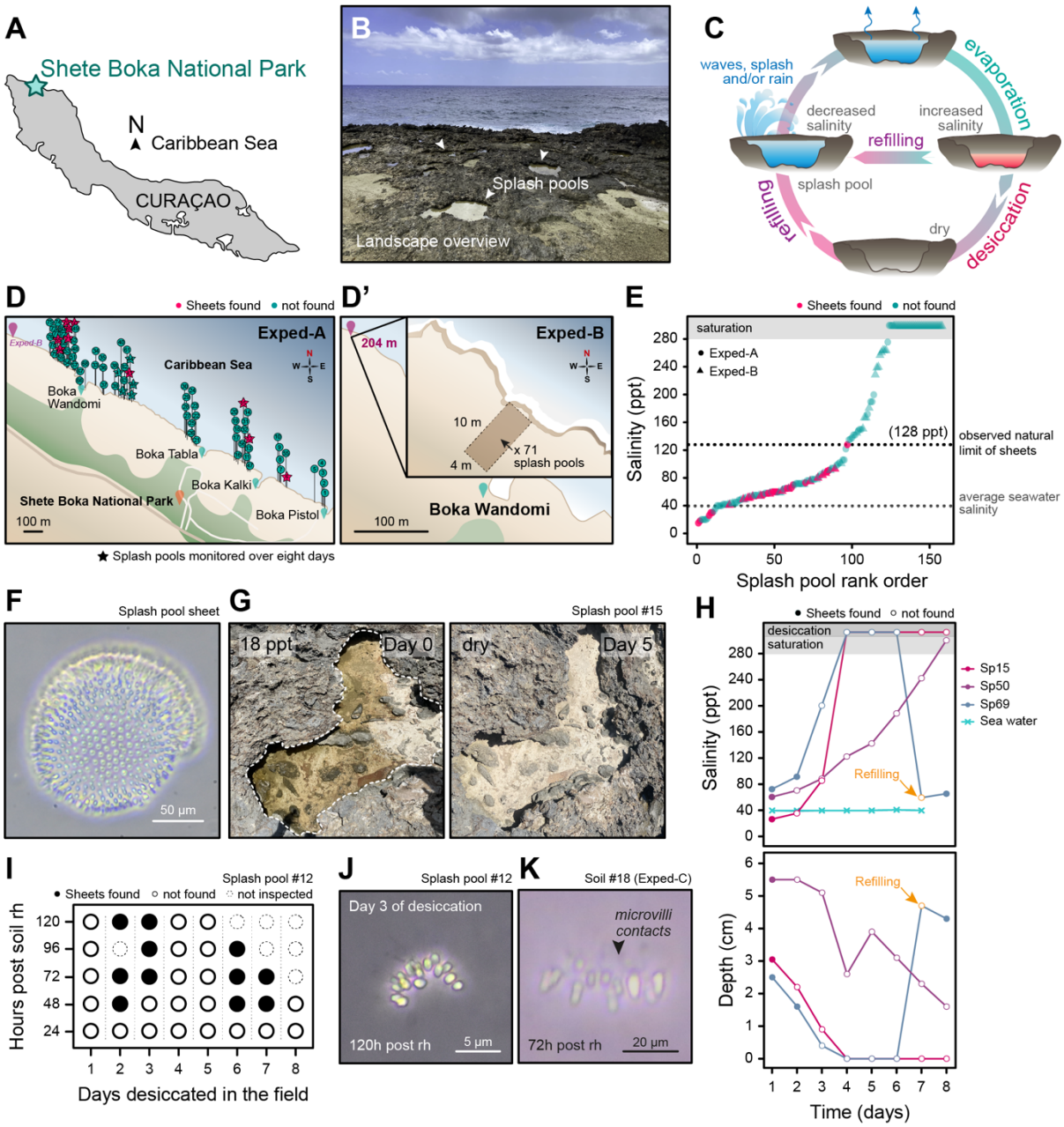

Figure 3. Natural evaporation-refilling cycles constrain the occurrence of multicellular *C. flexa* in the wild.

(A) Map of Curaçao and location of Shete Boka National Park (turquoise star) where fieldwork data was collected in Exped-A, Exped-B and Exped-C expeditions (12° 22' 5.718" N, 69° 06' 56.916" W). (B) Representative photograph of the landscape in Shete Boka, including splash pools where *C. flexa* sheets can be found (white arrowheads). (C) Schematics of a splash pool natural cycle of seawater evaporation, desiccation, and refilling. (D) Maps showing the locations of sampled splash pools in Exped-A and in Exped-B expeditions. In Exped-A (D), samples were collected from splash pools along ~2 km of Shete Boka coastline (n=79). 15 of these splash pools were randomly selected for daily monitoring during eight days (stars) (shown are results from the first day of monitoring). Colors indicate whether sheets were found (magenta) or not found (turquoise) upon microscopic inspection. In Exped-B (D'), a random number generator was used to select the randomized sampling location (purple pin,

204 m upstream of Boka Wandomi). Samples were collected from splash pools within an area of 10 m by 4 m (n=71). (E) Distribution of salinity of splash pools surveyed in Exped-A (circles) and Exped-B (triangles). For daily monitored splash pools, measurements from the first day of monitoring are shown, except for those where sheets were observed more than one day. In that case, the minimum and maximum salinity values are reported. Magenta and turquoise colors indicate that sheets were respectively found and not found in splash pool samples. The observed natural limit of salinity where sheets were found (128 ppt) is indicated by an orange dotted line, and the average seawater salinity measured in the *bokas* with a gray dotted line. Gray area: salinity saturation (>280 ppt). (F) Brightfield image of a sheet observed in a splash pool sample. (G) Representative images of a splash pool near Boka Kalki (Sp15) followed for eight days, showing recorded salinity in the upper left. This splash pool was completely desiccated on day 5 (right). Dashed line: splash pool outline. (H) Salinity (upper panel) and depth (lower panel) measurements in three representative splash pools followed over eigth days. Shown are one splash pool that experienced evaporation but not complete desiccation (Sp50), one splash pool that experienced complete desiccation (Sp15), and one splash pool that experienced both desiccation and refilling (Sp69). Filled and empty circles indicate that sheets were respectively found and not found in splash pool samples. Gray area: salinity saturation. Dashed lines: dry periods. Orange circles: refilling events. (I) Recovery of sheets from soil samples collected from a splash pool (Sp12) during its dry period in Exped-A. Soil samples were collected every day for eight days and were independently rehydrated in the laboratory with filtered seawater from the *bokas,* reconstituting salinity back to 42 ppt. Each rehydrated soil sample was monitored over five days for sheet re-appearance. Filled circle: sheets observed. Empty circle: sheets not observed. Dashed empty circle: sample not inspected. rh: rehydration. (J) Brightfield image of a soil-recovered sheet (same experiment as in I) collected after 3 days of desiccation and rehydrated in the laboratory. (K) Brigthfield image of a soil-recovered sheet independently collected and rehydrated from a splash pool sample (Soil #18) in Exped-C. Time post-rehydration in J-K is depicted in the lower left. Figure related to **Figures S4-S9**, **movies S14-S16**, **Tables S1-S2** and **Supplementary Files S1-S4**.

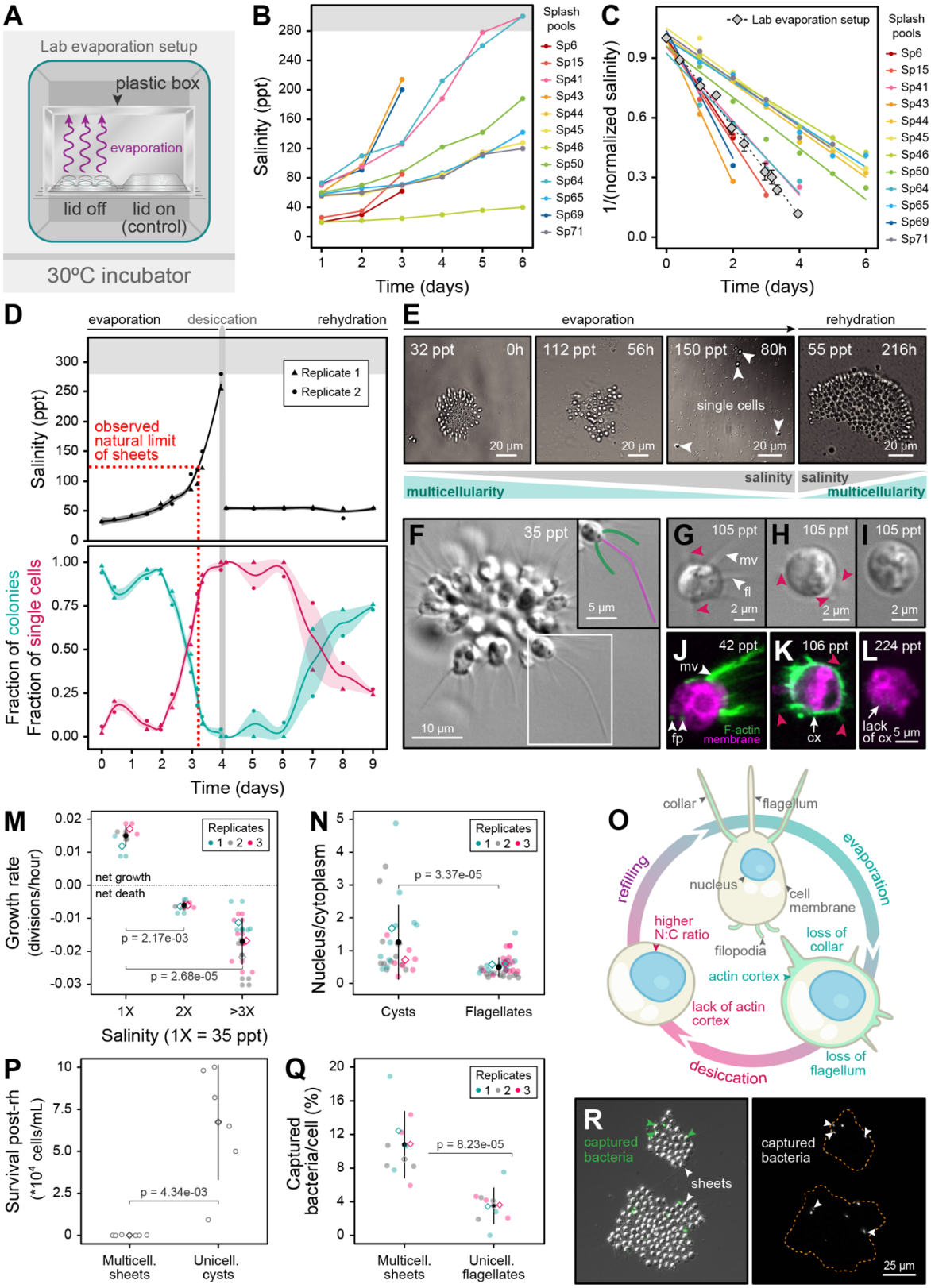

Figure 4. Experimental evaporation-refilling cycles cause reversible transitions in and out of multicellularity.

Figure 4. (A) Laboratory experimental evaporation setup in a 30ºC incubator. Note that plates were kept with the plate's lid off (gradual evaporation condition) or the plate lid's on (low-evaporation control) over a grid and were covered with a plastic box to avoid contamination and favour air exchange. (B) Salinity monitoring of followed-up splash pools during an 8-day time course from Exped-A expedition. Splash pools during the first 6 days of the time course gradually evaporated, and hence they were used to model splash pool evaporation dynamics. Splash pools with less than 3 points outside saturation range (gray area) were not included in the modelling (i.e. Sp12, Sp42, and Sp70; see **Figure S7**). (C) Normalized inverse of salinity over time during gradual evaporation comparing empirical data from splash pools in B versus the laboratory evaporation setup (gray) in A. (D) Quantification of salinity (upper panel) and fraction of cells in colonies (magenta) or in single cells (turquoise) (lower panel) during a 9-day gradual evaporation time course. Dark gray rectangle: complete desiccation (dry period). Orange dotted line: observed natural salinity limit of sheet occurrence. Gray area: salinity saturation. Lines correspond to mean values and shadowed area to standard deviation. Experiment performed on two independent biological replicates. (E) Stills of C. flexa sheets during the same 9-day gradual evaporation timecourse in D, showing salinity (in ppt, upper left) and time (upper right). Sheets had completely dissociated into single cells (white arrowheads) after 80 hours of gradual evaporation. Multicellular sheets were observed again after complete desiccation and rehydration with 1X ASW. (F-I) Brightfield images of C. flexa showing morphological changes during gradual evaporation, showing salinity (in ppt, upper right). At ~1X seawater salinity (F), C. flexa occurs in the form of multicellular sheets of flagellated cells (white square). Green pseudocolor: collar. Magenta pseudocolor: flagellum. During gradual evaporation (G-I), sheets dissociate into unicellular cysts. Cysts often lack a collar of microvilli (mv), often lack a flagellum (fl), and can exhibit filopodia-like protrusions (magenta arrowheads). (J-L) AiryScan micrographs of C. flexa cells fixed during gradual evaporation stained with a membrane (FMTM 4-64FX, magenta) and F-actin (phalloidin Alexa 488, green) dyes, showing salinity (in ppt, upper right). A flagellate cell (J, low-evaporation control) exhibits distribution of F-actin in the collar of microvilli (mv, white arrowhead) and filopodia (fp, white arrowhead). Gradual evaporation triggers a morphological change from a flagellate to a cyst, showing filopodia-like protrusions (magenta arrowheads) and a transient actin cortex (cx) at early stages of evaporation (K, white arrow) which disappears as salinity approaches saturation (L). (M) Growth rate of cells at different salinities during gradual evaporation in three independent biological replicates. Black circles: mean. Error bars: standard deviation. n=28, p by the Mann-Whitney U test. Diamonds: mean values of independent biological replicates. (N) Quantification of the nucleus-to-cytoplasm ratio in cysts (n=27) and flagellates (n=38) in three independent biological replicates. Black circles: means. Error bars: standard deviations. Diamonds: mean values of independent biological replicates. p by the Mann-Whitney U test. (O) Schematic summarizing phenotypic changes experienced by C. flexa cells during gradual evaporation. At early stages of evaporation (turquoise), flagellate cells differentiate into cysts by losing their collar and flagellum and show a temporal actin cortex. At later stages of evaporation (desiccation, magenta), cysts lack an actin cortex and show a higher nucleus-to-cytoplasm ratio. Rehydration (refilling, purple) induces a cyst-to-flagellate cell transition, where cells regenerate their collar and flagellum and re-form multicellular sheets. (P) Quantification of cell survival after 12 hours of desiccation in multicellular sheets (n=6 technical replicates) to unicellular cysts (n=6 technical replicates). Diamonds: means. Error bars: standard deviations. p by the Mann-Whitney U test. (Q) C. flexa multicellular sheets are more efficient at capturing bacteria than unicellular flagellates. Number of labelled bacteria captured per flagellate cells in multicellular colonies (n=9) or in cultures of unicellular flagellates (n=9) in three independent biological replicates. Black circles: means. Error bars: standard deviations. Diamonds: means of independent biological replicates. p by the Mann-Whitney U test. (R) DIC images of multicellular sheets (upper panel, white arrowheads) capturing fluorescently labelled bacteria using Bactoview dye (upper panel: green; lower panel: white). Figure related to **Figures S9-S14** and **movies S17-S18.**

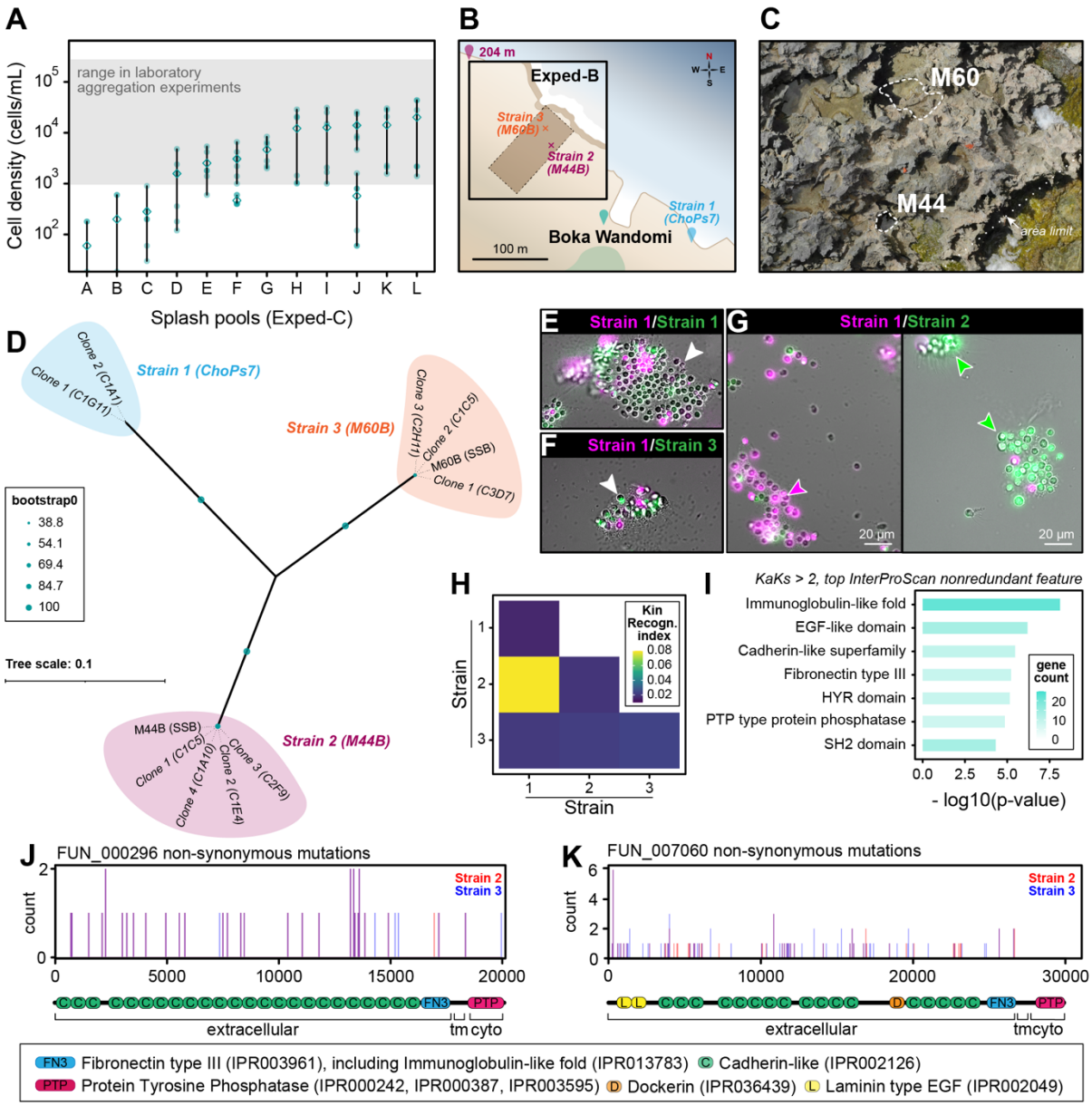

Figure 5. Aggregation of *C. flexa* is compatible with cell densities measured in the field and is constrained by kin recognition between genetically different strains.

(A) Cell density in nature is sufficient for aggregation. Cell density measured in 12 splash pools (A to L) compared to the range used in laboratory aggregation experiments (gray area). Diamonds are the average estimate, and bars indicate uncertainty (ranging from minimal to maximal possible estimated values). (B) Source location of the three distinct strains of *C. flexa* used in kin recognition experiments. (C) Aerial view of two neighboring splash pools in the Exped-B site, M44 and M60, from which strains 2 and 3 were respectively isolated. (D) Phylogenomic tree of strains 1, 2 and 3, including single-sheet-bottleneck cultures (SSB) and three to four single-cell bottlenecked clones from each strain. (E) Cells of the same strain (here strain 1), marked with magenta or green fluorophores, readily aggregate together regardless of color, resulting in dual-colored colonies (white arrowhead; compare Fig. 2). (F) Cells of strains 1 and 3 (clone 1), marked with distinct fluorophores, readily aggregate into chimeric sheets (white arrowhead). (G) Cells of strains 1 and 2 (clone 1), marked with distinct fluorophores, preferentially aggregate with their own strain, resulting in colonies with little or no chimerism (magenta and green arrowheads). This indicates kin recognition. (H) Quantification of kin recognition in different

727 pairwise strain combinations (see **Figure S15A-C** and Methods). The kin recognition index is calculated
728 based on the variance of the proportion of green (or red) cells across sheets for a given combination of
729 strains (as in[143]). A unimodal distribution centred around a median peak at 50% indicates no kin
730 discrimination, while a bimodal distribution with two distinct peaks (and thus with higher variance)
731 indicates kin discrimination (see Methods). All experiments were performed in two independent
732 biological replicates. p = 4.6e-3 by a one-way ANOVA. (I) Nonredundant top InterProScan domain
733 annotations enriched in candidate kin recognition loci (identified by high Ka/Ks ratio). See **Figure S17**
734 for full list. (J) Four polymorphic candidate kin recognition loci encoding transmembrane proteins with
735 potential roles in cell-cell adhesion and signalling. Upper row: number of coding differences (aminoacid
736 substitutions) between the strain of interest (2 or 3) compared to strain 1. Lower row: domain
737 architecture predicted with InterProScan (see domains legend), highlighting non-cytoplasmic,
738 cytoplasmic (cyto) and transmembrane (tm) regions.

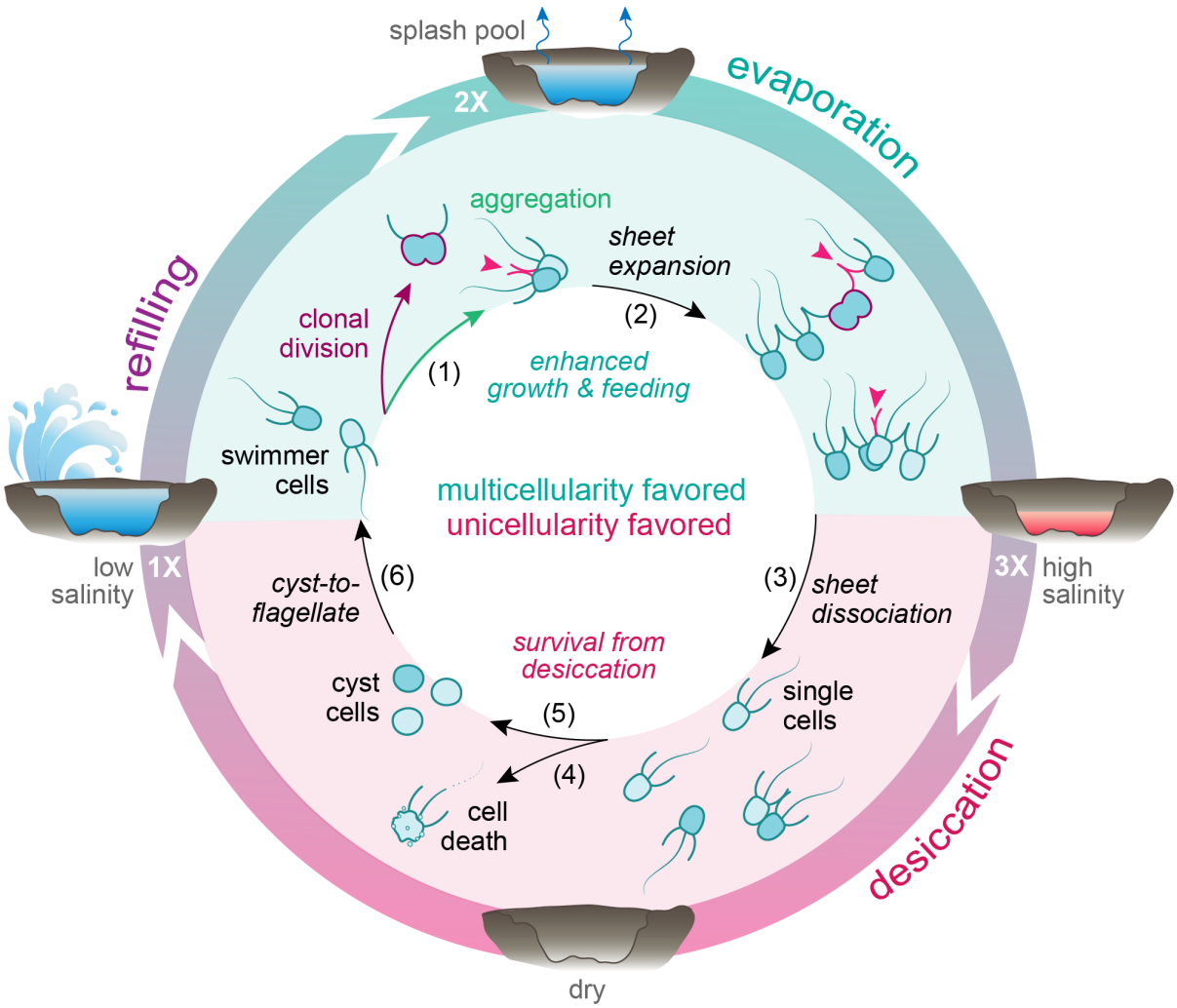

Figure 6. The environmentally entrained clonal-aggregative life cycle of *C. flexa*

Summary schematic of *C. flexa* mixed clonal-aggregative development entrained by natural splash pool evaporation-refilling cycles. Multicellularity is favoured in low salinity, where sheets exhibit enhanced growth and prey capture (turquoise): (1) unicellular flagellate cells can aggregate and/or divide clonally to initiate multicellular sheet development, maintaining direct cell-cell adhesions in their collar (orange arrowheads); (2) sheets expand by clonal cell division, by aggregation of individual cells, and by sheet fusion. Gradual evaporation leads to increase in salinity and favours unicellularity (magenta): (3) *C. flexa* remains multicellular in up to 3-fold salinity, but hypersaline conditions (>3-fold salinity) trigger sheet dissociation into single cells that are incapable of proliferation and occasionally to cell death (4). Gradual evaporation, instead, results in the differentiation of flagellates into cysts (5) capable of surviving desiccation. (6) Rehydration restores permissive salinity and induces differentiation of cysts into flagellates, which undergo clonal-aggregative multicellular development.

References

1. Grosberg, R. K. & Strathmann, R. R. The Evolution of Multicellularity: A Minor Major Transition? *Annu. Rev. Ecol. Evol. Syst.* **38**, 621–654 (2007).
2. Sebé-Pedrós, A., Degnan, B. M. & Ruiz-Trillo, I. The origin of Metazoa: a unicellular perspective. *Nat. Rev. Genet.* (2017) doi:10.1038/nrg.2017.21.
3. Bonner, J. T. The origins of multicellularity. *Integrative Biology* **1**, 27–36 (1998).
4. Brunet, T. & King, N. The Origin of Animal Multicellularity and Cell Differentiation. *Dev. Cell* **43**, 124–140 (2017).
5. Staps, M., Van Gestel, J. & Tarnita, C. E. Emergence of diverse life cycles and life histories at the origin of multicellularity. *Nat Ecol Evol* **3**, 1197–1205 (2019).
6. Márquez-Zacarías, P., Conlin, P. L., Tong, K., Pentz, J. T. & Ratcliff, W. C. Why have aggregative multicellular organisms stayed simple? *Curr Genet* **67**, 871–876 (2021).
7. Schaap, P. Eukaryote Aggregative Multicellularity: Phylogenetic Distribution and a Case Study of Its Proximate and Ultimate Cause in Dictyostelia. in *The Evolution of Multicellularity* (CRC Press, 2022).
8. Leger, M. M. & Ruiz-Trillo, I. Phylogenetics of Clonal Multicellularity. in *The Evolution of Multicellularity* (CRC Press, 2022).
9. Fisher, R. M., Cornwallis, C. K. & West, S. A. Group Formation, Relatedness, and the Evolution of Multicellularity. *Current Biology* **23**, 1120–1125 (2013).
10. Fairclough, S. R., Dayel, M. J. & King, N. Multicellular development in a choanoflagellate. *Curr. Biol.* **20**, R875-876 (2010).
11. Leadbeater, B. S. C. *The Choanoflagellates: Evolution, Biology and Ecology*. (Cambridge University Press, 2014).
12. King, N. The unicellular ancestry of animal development. *Dev. Cell* **7**, 313–325 (2004).
13. Brunet, T. *et al.* Light-regulated collective contractility in a multicellular choanoflagellate. *Science* **366**, 326–334 (2019).
14. Mehdiabadi, N. J., Kronforst, M. R., Queller, D. C. & Strassmann, J. E. Phylogeny, reproductive isolation and kin recognition in the social amoeba Dictyostelium purpureum. *Evolution* **63**, 542–548 (2009).
15. Ho, H.-I., Hirose, S., Kuspa, A. & Shaulsky, G. Kin recognition protects cooperators against cheaters. *Curr Biol* **23**, 1590–1595 (2013).
16. Chaine, A. S., Schtickzelle, N., Polard, T., Huet, M. & Clobert, J. Kin-based recognition and social aggregation in a ciliate. *Evolution* **64**, 1290–1300 (2010).
17. Benabentos, R. *et al.* Polymorphic members of the lag gene family mediate kin discrimination in Dictyostelium. *Curr. Biol.* **19**, 567–572 (2009).
18. Lamża, Ł. Diversity of 'simple' multicellular eukaryotes: 45 independent cases and six types of multicellularity. *Biological Reviews* **98**, 2188–2209 (2023).
19. Velicer, M. L. F., Kaitlin A. Schaal, Gregory J. Group Formation: On the Evolution of Aggregative Multicellularity. in *The Evolution of Multicellularity* (CRC Press, 2022).
20. Ros-Rocher, N., Pérez-Posada, A., Leger, M. M. & Ruiz-Trillo, I. The origin of animals: an ancestral reconstruction of the unicellular-to-multicellular transition. *Open Biology* **11**, 200359 (2021).
21. Booth, D. S. & King, N. The history of Salpingoeca rosetta as a model for reconstructing animal origins. in *Current Topics in Developmental Biology* vol. 147 73–91 (Elsevier, 2022).
22. Ros-Rocher, N. & Brunet, T. What is it like to be a choanoflagellate? Sensation, processing and behavior in the closest unicellular relatives of animals. *Anim Cogn* **26**, 1767–1782 (2023).
23. Carr, M., Leadbeater, B. S. C., Hassan, R., Nelson, M. & Baldauf, S. L. Molecular phylogeny of choanoflagellates, the sister group to Metazoa. *Proc. Natl. Acad. Sci. U.S.A.* **105**, 16641–16646 (2008).
24. Leadbeater, B. S. C. *The Choanoflagellates: Evolution, Biology and Ecology*. (Cambridge University Press, Cambridge, 2015). doi:10.1017/CBO9781139051125.
25. Brunet, T. & King, N. The Origin of Animal Multicellularity and Cell Differentiation. *Developmental Cell* **43**, 124–140 (2017).
26. Fairclough, S. R., Dayel, M. J. & King, N. Multicellular development in a choanoflagellate. *Current Biology* **20**, R875–R876 (2010).
27. Fairclough, S. R. *et al.* Premetazoan genome evolution and the regulation of cell differentiation in the choanoflagellate Salpingoeca rosetta. *Genome Biology* **14**, R15 (2013).

28. Dayel, M. J. *et al.* Cell differentiation and morphogenesis in the colony-forming choanoflagellate *Salpingoeca rosetta*. *Developmental Biology* **357**, 73–82 (2011).
29. Haeckel, E. & Wright, E. P., F. L. S. Memoirs: The Gastraea-Theory, the Phylogenetic Classification of the Animal Kingdom and the Homology of the Germ-Lamellæ. *Journal of Cell Science* **s2-14**, 223–247 (1874).
30. Nielsen, C. Six major steps in animal evolution: are we derived sponge larvae? *Evol Dev* **10**, 241–257 (2008).
31. Arendt, D., Benito-Gutierrez, E., Brunet, T. & Marlow, H. Gastric pouches and the mucociliary sole: setting the stage for nervous system evolution. *Philosophical Transactions of the Royal Society B: Biological Sciences* **370**, 20150286 (2015).
32. Hehenberger, E. *et al.* Novel Predators Reshape Holozoan Phylogeny and Reveal the Presence of a Two-Component Signaling System in the Ancestor of Animals. *Curr Biol* **27**, 2043-2050.e6 (2017).
33. Sebé-Pedrós, A. *et al.* Regulated aggregative multicellularity in a close unicellular relative of metazoa. *eLife* **2**, e01287 (2013).
34. Mylnikov, A. P., Tikhonenkov, D. V., Karpov, S. A. & Wylezich, C. Microscopical Studies on *Ministeria vibrans* Tong, 1997 (Filasterea) Highlight the Cytoskeletal Structure of the Common Ancestor of Filasterea, Metazoa and Choanoflagellata. *Protist* **170**, 385–396 (2019).
35. Tikhonenkov, D. V. *et al.* New Lineage of Microbial Predators Adds Complexity to Reconstructing the Evolutionary Origin of Animals. *Current Biology* **30**, 4500-4509.e5 (2020).
36. Bonner, J. T. Aggregation and Differentiation in the Cellular Slime Molds. *Annual Review of Microbiology* **25**, 75–92 (1971).
37. Du, Q., Kawabe, Y., Schilde, C., Chen, Z. & Schaap, P. The Evolution of Aggregative Multicellularity and Cell–Cell Communication in the Dictyostelia. *Journal of Molecular Biology* **427**, 3722–3733 (2015).
38. Shah, H. *et al.* Life-cycle-coupled evolution of mitosis in close relatives of animals. *Nature* **630**, 116–122 (2024).
39. Olivetta, M., Bhickta, C., Chiaruttini, N., Burns, J. & Dudin, O. A multicellular developmental program in a close animal relative. Preprint at https://doi.org/10.1101/2024.03.25.586530 (2024).
40. Shabardina, V. *et al.* Ichthyosporea: a window into the origin of animals. *Commun Biol* **7**, 915 (2024).
41. Brunet, T. *et al.* Light-regulated collective contractility in a multicellular choanoflagellate. *Science* **366**, 326–334 (2019).
42. Brunet, T. & Booth, D. S. Cell polarity in the protist-to-animal transition. in *Current Topics in Developmental Biology* S0070215323000455 (Elsevier, 2023). doi:10.1016/bs.ctdb.2023.03.001.
43. Reyes-Rivera, J. *et al.* Nitric oxide signaling controls collective contractions in a colonial choanoflagellate. *Current Biology* **32**, 2539-2547.e5 (2022).
44. Ros-Rocher, N. *et al.* Chemical factors induce aggregative multicellularity in a close unicellular relative of animals. *Proc. Natl. Acad. Sci. U.S.A.* **120**, e2216668120 (2023).
45. Keller, E. F. & Segel, L. A. Initiation of slime mold aggregation viewed as an instability. *Journal of Theoretical Biology* **26**, 399–415 (1970).
46. Leadbeater, B. S. Life-history and ultrastructure of a new marine species of Proterospongia (Choanoflagellida). *Journal of the Marine Biological Association of the United Kingdom* **63**, 135–160 (1983).
47. Little, C. & Kitching, J. A. *The Biology of Rocky Shores*. (Oxford University Press, 1996).
48. Garbary, D. The Margin of the Sea. in *Algae and Cyanobacteria in Extreme Environments* (ed. Seckbach, J.) 173–191 (Springer Netherlands, Dordrecht, 2007). doi:10.1007/978-1-4020-6112-7_9.
49. Huggett, J. & Griffiths, C. Some relationships between elevation, physico-chemical variables and biota of intertidal rock pools. *Mar. Ecol. Prog. Ser.* **29**, 189–197 (1986).
50. Amsalem, E. & Rilov, G. High thermal plasticity, and vulnerability, in extreme environments at the warm distributional edge: The case of a tidepool shrimp. *Journal of Experimental Marine Biology and Ecology* **545**, 151641 (2021).
51. Davison, I. R. & Pearson, G. A. Stress Tolerance in Intertidal Seaweeds. *Journal of Phycology* **32**, 197–211 (1996).
52. Stein, F. *Der Organismus Der Infusionsthiere*. (W. Engelmann, Leipzig, 1859). doi:10.5962/bhl.title.3933.
53. Saville-Kent, W. *A Manual of the Infusoria : Including a Description of All Known Flagellate, Ciliate, and Tentaculiferous Protozoa, British and Foreign, and an Account of the Organization and the Affinities of the Sponges*. (D. Bogue, London, 1880). doi:10.5962/bhl.title.10143.

54. Reess, M. & Fisch, C. *Untersuchungen über bau und Lebensgeschichte der Hirschtrüffel, Elaphomyces*. (T. Fischer, 1887).
55. Leadbeater, B. S. C. & Karpov, S. A. Cyst Formation in a Freshwater Strain of the Choanoflagellate Desmarella moniliformis Kent. *Journal of Eukaryotic Microbiology* **47**, 433–439 (2000).
56. Stoupin, D. *et al.* Cryptic diversity within the choanoflagellate morphospecies complex *Codosiga botrytis* – Phylogeny and morphology of ancient and modern isolates. *European Journal of Protistology* **48**, 263–273 (2012).
57. Jeuck, A., Arndt, H. & Nitsche, F. Extended phylogeny of the Craspedida (Choanomonada). *European Journal of Protistology* **50**, 430–443 (2014).
58. Venter, P. C., Nitsche, F. & Arndt, H. The Hidden Diversity of Flagellated Protists in Soil. *Protist* **169**, 432–449 (2018).
59. Elsas, J. D. van, Trevors, J. T., Rosado, A. S. & Nannipieri, P. *Modern Soil Microbiology, Third Edition*. (CRC Press, 2019).
60. Brunet, T. *et al.* A flagellate-to-amoeboid switch in the closest living relatives of animals. *eLife* **10**, e61037 (2021).
61. Li, Y., Wang, Y., Zhang, S., Maurer-Alcalá, X. X. & Yan, Y. How Ciliated Protists Survive by Cysts: Some Key Points During Encystment and Excystment. *Frontiers in Microbiology* **13**, (2022).
62. Schaap, P. & Schilde, C. Encystation: the most prevalent and underinvestigated differentiation pathway of eukaryotes. *Microbiology* **164**, 727–739 (2018).
63. Verni, F. & Rosati, G. Resting cysts: A survival strategy in Protozoa Ciliophora. *Italian Journal of Zoology* **78**, 134–145 (2011).
64. Griffiths, A. J. Encystment in Amoebae. in *Advances in Microbial Physiology* (eds. Rose, A. H. & Wilkinson, J. F.) vol. 4 105–129 (Academic Press, 1969).
65. Gong, Z.-W., Fan, X.-P., Ma, R. & Ni, B. Ultrastructure of vegetative cells and resting cysts, and live observations of the encystation and excystation processes in Diophrys oligothrix Borror, 1965 (Protista, Ciliophora). *Journal of Morphology* **279**, 1397–1407 (2018).
66. Bowers, B. & Korn, E. D. THE FINE STRUCTURE OF ACANTHAMOEBA CASTELLANII (NEFF STRAIN) : II. Encystment. *Journal of Cell Biology* **41**, 786–805 (1969).
67. Corliss, J. O. & Esser, S. C. Comments on the Role of the Cyst in the Life Cycle and Survival of Free-Living Protozoa. *Transactions of the American Microscopical Society* **93**, 578–593 (1974).
68. Chen, F. *et al.* New contribution to the morphology and molecular mechanism of Euplotes encysticus encystment. *Sci Rep* **8**, 12795 (2018).
69. Grimes, G. W. Differentiation During Encystment and Excystment in Oxytricha fallax*. *The Journal of Protozoology* **20**, 92–104 (1973).
70. Atkins, M. S., Anderson, O. R. & Wirsen, C. O. Effect of hydrostatic pressure on the growth rates and encystment of flagellated protozoa isolated from a deep-sea hydrothermal vent and a deep shelf region. *Marine Ecology Progress Series* **171**, 85–95 (1998).
71. Di Ciano, C. *et al.* Osmotic stress-induced remodeling of the cortical cytoskeleton. *American Journal of Physiology-Cell Physiology* **283**, C850–C865 (2002).
72. Komis, G., Apostolakos, P. & Galatis, B. Hyperosmotic stress-induced actin filament reorganization in leaf cells of Chlorophyton comosum. *Journal of Experimental Botany* **53**, 1699–1710 (2002).
73. Rivero, F. *et al.* The role of the cortical cytoskeleton: F-actin crosslinking proteins protect against osmotic stress, ensure cell size, cell shape and motility, and contribute to phagocytosis and development. *Journal of Cell Science* **109**, 2679–2691 (1996).
74. Aizawa, H. *et al.* Hyperosmotic stress-induced reorganization of actin bundles in Dictyostelium cells over-expressing cofilin. *Genes to Cells* **4**, 311–324 (1999).
75. Khan, N. A., Iqbal, J. & Siddiqui, R. Stress Management in Cyst-Forming Free-Living Protists: Programmed Cell Death and/or Encystment. *BioMed Research International* **2015**, e437534 (2015).
76. Balachandra, S., Sarkar, S. & Amodeo, A. A. The Nuclear-to-Cytoplasmic Ratio: Coupling DNA Content to Cell Size, Cell Cycle, and Biosynthetic Capacity. *Annu Rev Genet* **56**, 165–185 (2022).
77. Fenchel, T. Filter-feeding in Colonial Protists. *Protist* **170**, 283–286 (2019).
78. Koehl, M. a. R. Selective factors in the evolution of multicellularity in choanoflagellates. *Journal of Experimental Zoology Part B: Molecular and Developmental Evolution* **336**, 315–326 (2021).
79. Cavalier-Smith, T. Origin of animal multicellularity: precursors, causes, consequences—the choanoflagellate/sponge transition, neurogenesis and the Cambrian explosion. *Philosophical Transactions of the Royal Society B: Biological Sciences* **372**, 20150476 (2017).

80. Kirkegaard, J. B. & Goldstein, R. E. Filter-feeding, near-field flows, and the morphologies of colonial choanoflagellates. *Phys. Rev. E* **94**, 052401 (2016).
81. L'Etoile, N. J. & King-Smith, C. Rosette Colonies of Choanoflagellates (Salpingoeca rosetta) Show Increased Food Vacuole Formation Compared with Single Swimming Cells. *Journal of Eukaryotic Microbiology* **67**, 263–267 (2020).
82. King, N. *et al.* The genome of the choanoflagellate Monosiga brevicollis and the origin of metazoans. *Nature* **451**, 783–788 (2008).
83. Fairclough, S. R. *et al.* Premetazoan genome evolution and the regulation of cell differentiation in the choanoflagellate Salpingoeca rosetta. *Genome Biol* **14**, R15 (2013).
84. Hirose, S., Benabentos, R., Ho, H.-I., Kuspa, A. & Shaulsky, G. Self-recognition in social amoebae is mediated by allelic pairs of tiger genes. *Science* **333**, 467–470 (2011).
85. Tarnita, C. E., Taubes, C. H. & Nowak, M. A. Evolutionary construction by staying together and coming together. *Journal of Theoretical Biology* **320**, 10–22 (2013).
86. Tang, S., Pichugin, Y. & Hammerschmidt, K. An environmentally induced multicellular life cycle of a unicellular cyanobacterium. *Current Biology* **33**, 764-769.e5 (2023).
87. Mizuno, K. *et al.* Novel multicellular prokaryote discovered next to an underground stream. *eLife* **11**, e71920 (2022).
88. Barrere, J., Nanda, P. & Murray, A. W. Alternating selection for dispersal and multicellularity favors regulated life cycles. *Current Biology* **33**, 1809-1817.e3 (2023).
89. Pichugin, Y., Park, H. J. & Traulsen, A. Evolution of simple multicellular life cycles in dynamic environments. *J. R. Soc. Interface.* **16**, 20190054 (2019).
90. Staps, M., Van Gestel, J. & Tarnita, C. E. Life Cycles as a Central Organizing Theme for Studying Multicellularity. in *The Evolution of Multicellularity* (CRC Press, 2022).
91. Stanley, S. M. An Ecological Theory for the Sudden Origin of Multicellular Life in the Late Precambrian. *Proceedings of the National Academy of Sciences* **70**, 1486–1489 (1973).
92. Tong, K., Bozdag, G. O. & Ratcliff, W. C. Selective drivers of simple multicellularity. *Current Opinion in Microbiology* **67**, 102141 (2022).
93. Richter, D. J. & King, N. The Genomic and Cellular Foundations of Animal Origins. *Annual Review of Genetics* **47**, 509–537 (2013).
94. Kirkegaard, J. B. & Goldstein, R. E. Filter-feeding, near-field flows, and the morphologies of colonial choanoflagellates. *Phys. Rev. E* **94**, 052401 (2016).
95. Boraas, M. E., Seale, D. B. & Boxhorn, J. E. Phagotrophy by a flagellate selects for colonial prey: A possible origin of multicellularity. *Evolutionary Ecology* **12**, 153–164 (1998).
96. Chin, N. E. *et al.* Formation of multicellular colonies by choanoflagellates increases susceptibility to capture by amoeboid predators. *Journal of Eukaryotic Microbiology* **70**, e12961 (2023).
97. Kumler, W. E., Jorge, J., Kim, P. M., Iftekhar, N. & Koehl, M. a. R. Does Formation of Multicellular Colonies by Choanoflagellates Affect Their Susceptibility to Capture by Passive Protozoan Predators? *Journal of Eukaryotic Microbiology* **67**, 555–565 (2020).
98. Roper, M., Dayel, M. J., Pepper, R. E. & Koehl, M. a. R. Cooperatively generated stresslet flows supply fresh fluid to multicellular choanoflagellate colonies. *Phys. Rev. Lett.* **110**, 228104 (2013).
99. Short, M. B. *et al.* Flows driven by flagella of multicellular organisms enhance long-range molecular transport. *Proceedings of the National Academy of Sciences* **103**, 8315–8319 (2006).
100. Herron, M. D. *et al.* De novo origins of multicellularity in response to predation. *Sci Rep* **9**, 2328 (2019).
101. H. James-Clark A. B. IV.—Conclusive proofs of the animality of the ciliate sponges, and of their affinities with the Infusoria flagellata. *Annals and Magazine of Natural History* (1867) doi:10.1080/00222936708679703.
102. Hibberd, D. J. Observations on the ultrastructure of the choanoflagellate Codosiga botrytis (Ehr.) saville-kent with special reference to the flagellar apparatus. *Journal of Cell Science* **17**, 191–219 (1975).
103. Pettitt, M. E., Orme, B. A. A., Blake, J. R. & Leadbeater, B. S. C. The hydrodynamics of filter feeding in choanoflagellates. *European Journal of Protistology* **38**, 313 (2002).
104. Nagy, L. G., Varga, T., Csernetics, Á. & Virágh, M. Fungi took a unique evolutionary route to multicellularity: Seven key challenges for fungal multicellular life. *Fungal Biology Reviews* **34**, 151–169 (2020).
105. Brown, M. W., Spiegel, F. W. & Silberman, J. D. Phylogeny of the 'forgotten' cellular slime mold, Fonticula alba, reveals a key evolutionary branch within Opisthokonta. *Mol Biol Evol* **26**, 2699–2709 (2009).

106. Toret, C., Picco, A., Boiero-Sanders, M., Michelot, A. & Kaksonen, M. The cellular slime mold *Fonticula alba* forms a dynamic, multicellular collective while feeding on bacteria. *Current Biology* **32**, 1961-1973.e4 (2022).
107. Sauer, K. *et al.* The biofilm life cycle: expanding the conceptual model of biofilm formation. *Nat Rev Microbiol* **20**, 608–620 (2022).
108. Chavhan, Y., Dey, S. & Lind, P. A. Bacteria evolve macroscopic multicellularity by the genetic assimilation of phenotypically plastic cell clustering. *Nat Commun* **14**, 3555 (2023).
109. Kapsetakia, S. E., Tep, A. & West, S. A. How do algae form multicellular groups? *Evolutionary Ecology Research* **18**, 663–675 (2017).
110. Rose, C. J. & Hammerschmidt, K. What Do We Mean by Multicellularity? The Evolutionary Transitions Framework Provides Answers. *Front. Ecol. Evol.* **9**, 730714 (2021).
111. Pentz, J. T. *et al.* Evolutionary consequences of nascent multicellular life cycles. *eLife* **12**, e84336 (2023).
112. Hammerschmidt, K., Rose, C. J., Kerr, B. & Rainey, P. B. Life cycles, fitness decoupling and the evolution of multicellularity. *Nature* **515**, 75–79 (2014).
113. Michod, R. E. Evolution of individuality during the transition from unicellular to multicellular life. *Proc. Natl. Acad. Sci. U.S.A.* **104 Suppl 1**, 8613–8618 (2007).
114. Strassmann, J. E., Zhu, Y. & Queller, D. C. Altruism and social cheating in the social amoeba Dictyostelium discoideum. *Nature* **408**, 965–967 (2000).
115. Velicer, G. J., Kroos, L. & Lenski, R. E. Developmental cheating in the social bacterium Myxococcus xanthus. *Nature* **404**, 598–601 (2000).
116. Pentz, J. T. *et al.* Ecological Advantages and Evolutionary Limitations of Aggregative Multicellular Development. *Current Biology* **30**, 4155-4164.e6 (2020).
117. Knoll, A. H. The Multiple Origins of Complex Multicellularity. *Annual Review of Earth and Planetary Sciences* **39**, 217–239 (2011).
118. Márquez-Zacarías, P., Conlin, P. L., Tong, K., Pentz, J. T. & Ratcliff, W. C. Why have aggregative multicellular organisms stayed simple? *Curr Genet* **67**, 871–876 (2021).
119. Fisher, R. M., Cornwallis, C. K. & West, S. A. Group Formation, Relatedness, and the Evolution of Multicellularity. *Current Biology* **23**, 1120–1125 (2013).
120. Biernaskie, J. M. & West, S. A. Cooperation, clumping and the evolution of multicellularity. *Proceedings of the Royal Society B: Biological Sciences* **282**, 20151075 (2015).
121. Trunk, T., Khalil, H. S. & Leo, J. C. Bacterial autoaggregation. *AIMS Microbiol* **4**, 140–164 (2018).
122. Stratford, M. Lectin-mediated Aggregation of Yeasts — Yeast Flocculation. *Biotechnology and Genetic Engineering Reviews* **10**, 283–342 (1992).
123. Kessin, R. H., Gundersen, G. G., Zaydfudim, V. & Grimson, M. How cellular slime molds evade nematodes. *Proceedings of the National Academy of Sciences* **93**, 4857–4861 (1996).
124. Du, Q., Kawabe, Y., Schilde, C., Chen, Z.-H. & Schaap, P. The Evolution of Aggregative Multicellularity and Cell-Cell Communication in the Dictyostelia. *J. Mol. Biol.* **427**, 3722–3733 (2015).
125. Brown, M. W. & Silberman, J. D. The Non-dictyostelid Sorocarpic Amoebae. in *Dictyostelids* (eds. Romeralo, M., Baldauf, S. & Escalante, R.) 219–242 (Springer Berlin Heidelberg, Berlin, Heidelberg, 2013). doi:10.1007/978-3-642-38487-5_12.
126. Brown, M. W., Kolisko, M., Silberman, J. D. & Roger, A. J. Aggregative multicellularity evolved independently in the eukaryotic supergroup Rhizaria. *Curr Biol* **22**, 1123–1127 (2012).
127. Curtis, P. D., Taylor, R. G., Welch, R. D. & Shimkets, L. J. Spatial Organization of Myxococcus xanthus during Fruiting Body Formation. *J Bacteriol* **189**, 9126–9130 (2007).
128. Queller, D. C., Ponte, E., Bozzaro, S. & Strassmann, J. E. Single-Gene Greenbeard Effects in the Social Amoeba Dictyostelium discoideum. *Science* **299**, 105–106 (2003).
129. Gruenheit, N. *et al.* A polychromatic 'greenbeard' locus determines patterns of cooperation in a social amoeba. *Nat Commun* **8**, 14171 (2017).
130. Benabentos, R. *et al.* Polymorphic Members of the lag Gene Family Mediate Kin Discrimination in Dictyostelium. *Current Biology* **19**, 567–572 (2009).
131. Li, S. I. & Purugganan, M. D. The cooperative amoeba: Dictyostelium as a model for social evolution. *Trends in Genetics* **27**, 48–54 (2011).
132. Espinosa, A. & Paz-y-Miño-C, G. Evidence of taxa-, clone-, and kin-discrimination in protists: ecological and evolutionary implications. *Evol Ecol* **28**, 1019–1029 (2014).
133. Smith, J., Strassmann, J. E. & Queller, D. C. Fine-scale spatial ecology drives kin selection relatedness among cooperating amoebae. *Evolution* **70**, 848–859 (2016).

134. West, S. A., Griffin, A. S. & Gardner, A. Social semantics: altruism, cooperation, mutualism, strong reciprocity and group selection. *J of Evolutionary Biology* **20**, 415–432 (2007).
135. Haag, C. R., Riek, M., Hottinger, J. W., Pajunen, V. I. & Ebert, D. Founder events as determinants of within-island and among-island genetic structure of Daphnia metapopulations. *Heredity* **96**, 150–158 (2006).
136. Black, A. J., Bourrat, P. & Rainey, P. B. Ecological scaffolding and the evolution of individuality. *Nat Ecol Evol* **4**, 426–436 (2020).
137. Brunet, T. & King, N. The Single-Celled Ancestors of Animals: A History of Hypotheses. in *The evolution of multicellularity* (CRC Press, 2022).
138. Ferrer-Bonet, M. & Ruiz-Trillo, I. Capsaspora owczarzaki. *Current Biology* **27**, R829–R830 (2017).
139. Ocaña-Pallarès, E. *et al.* Divergent genomic trajectories predate the origin of animals and fungi. *Nature* **609**, 747–753 (2022).
140. Grau-Bové, X. *et al.* Dynamics of genomic innovation in the unicellular ancestry of animals. *Elife* **6**, e26036 (2017).
141. King, N. *et al.* The genome of the choanoflagellate Monosiga brevicollis and the origin of metazoans. *Nature* **451**, 783–788 (2008).
142. Torruella, G. *et al.* Phylogenomics Reveals Convergent Evolution of Lifestyles in Close Relatives of Animals and Fungi. *Curr Biol* **25**, 2404–2410 (2015).
143. Ostrowski, E. A., Katoh, M., Shaulsky, G., Queller, D. C. & Strassmann, J. E. Kin Discrimination Increases with Genetic Distance in a Social Amoeba. *PLoS Biol* **6**, e287 (2008).